

# 1 Carbon export and burial pathways driven by a low-latitude arc- 2 continent collision

3 Amy I. Hsieh<sup>1</sup>, Thierry Adatte<sup>1</sup>, Shraddha Band<sup>2</sup>, Li Lo<sup>3</sup>, Romain Vaucher<sup>4</sup>, Brahim Samba Bomou<sup>1</sup>,  
4 Laszlo Kocsis<sup>5</sup>, Pei-Ling Wang<sup>6</sup>, Samuel Jaccard<sup>1</sup>

5 <sup>1</sup>Institute of Earth Sciences, University of Lausanne, Lausanne, CH-1015, Switzerland

6 <sup>2</sup>Biodiversity Research Center, Academia Sinica, Taipei, 115, Taiwan

7 <sup>3</sup>Department of Geosciences, National Taiwan University, Taipei, 106, Taiwan

8 <sup>4</sup>College of Science and Engineering, James Cook University, Townsville, 4814, Australia

9 <sup>5</sup>Institute of Earth Surface Dynamics, University of Lausanne, Lausanne, CH-1015, Switzerland

10 <sup>6</sup>Institute of Oceanography, National Taiwan University, Taipei, 106, Taiwan

11 *Correspondence to:* Amy I. Hsieh (hsiehiamy@gmail.com)

12 **Abstract.** Chemical weathering of silicate rocks of low-latitude arc–continent collisions has been hypothesized as a driver of  
13 global cooling since the Neogene. In mid- to low-latitude regions, monsoon and tropical cyclone precipitation also drive  
14 intense physical erosion that contribute to terrestrial carbon export and nutrient-stimulated marine productivity. Despite this,  
15 the role of physical weathering erosion on carbon sequestration has largely been overlooked. To address this gap, we analyse  
16 late Miocene–early Pleistocene sedimentary and geochemical records from the Taiwan Western Foreland Basin and time-  
17 equivalent records from the northern South China Sea.

18 Along the continental slope, organic carbon is largely marine in origin, and its accumulation is largely controlled by long-  
19 term sea-level fall and glaciationshoreline progradation. In contrast, on the continental rise, organic carbon burial is  
20 controlled by high sedimentation rates related to Taiwan’s uplift and erosion (since ~5.4 Ma). Despite increased terrestrial  
21 erosion of Taiwan, the organic material remains mainly marine in origin, suggesting that primary production was enhanced  
22 along the coast by nutrient exported from Taiwan. Marine organic matter along Taiwan’s shore was subsequently  
23 remobilized by turbidity currents through submarine canyon systems and accumulating on the continental rise of Eurasia.  
24 The onset of Northern Hemisphere Glaciation (~3 Ma) and subsequent intensification of the East Asian Summer Monsoon  
25 during interglacial periods, and persistent tropical cyclone activity all further amplified nutrient export across the basin,  
26 further stimulating marine primary production.

27 Our findings demonstrate that arc–continent collision influences carbon sequestration through two pathways: (1) direct burial  
28 of terrestrial organic matter and (2) nutrient-fuelled marine productivity and burial. This work establishes a direct link  
29 between the erosion of an arc-continent collision and long-term carbon burial in adjacent ocean basins.

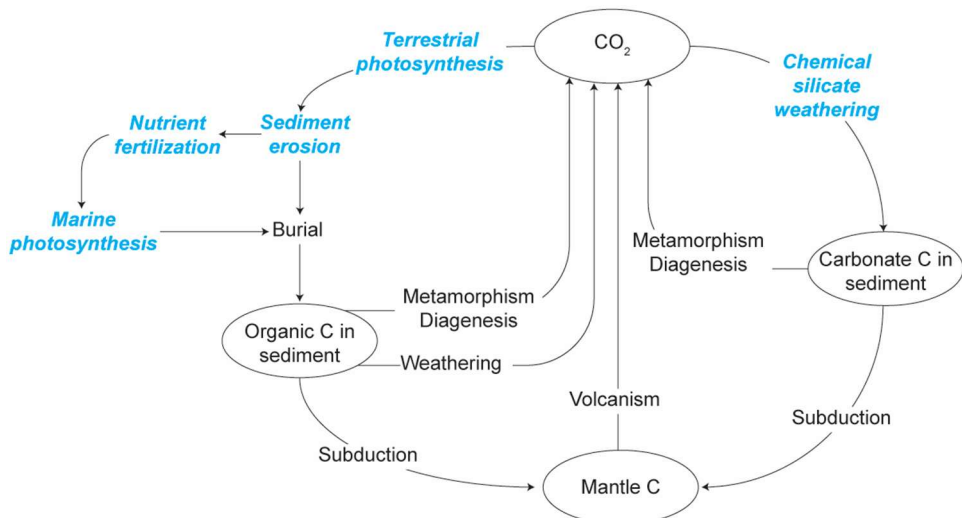
30 **1 Introduction**

31 Global cooling since the late Eocene has traditionally been attributed to tectonic forcing and enhanced chemical weathering  
32 of silicate rock from the Himalayan and Tibetan Plateau (Raymo and Ruddiman, 1992), which results in the removal of  
33 atmospheric CO<sub>2</sub> (Walker et al., 1981). However, weathering fluxes have decreased in both regions during the Neogene  
34 (Clift and Jonell, 2021; Clift et al., 2024a), and global silicate fluxes appear to have remained near steady-state through the  
35 Cenozoic (Caves et al., 2016) even as global cooling continued. To reconcile stable or declining chemical weathering rates  
36 with decreasing atmospheric CO<sub>2</sub>, an alternative hypothesis emphasized chemical erosion of arc-continent collisional  
37 orogens in low-latitude, tropical regions (Clift et al., 2024b; Jagoutz et al., 2016; Macdonald et al., 2019; Bayon et al., 2023).  
38 In such environments, warm and humid conditions amplify chemical weathering, enhancing carbon removal and  
39 sequestration. While existing studies support a correlation between the growth and weathering of low-latitude orogens and  
40 long-term atmospheric CO<sub>2</sub> concentration and global temperature records, they have yet to fully account for the roles of  
41 physical erosion, terrestrial organic carbon burial, and changes in marine productivity.

42 In low-latitude regions, tropical cyclones and monsoons are the primary drivers of erosion and sediment dispersal, delivering  
43 elevated sediment loads to adjacent seas via intense precipitation and high river discharge from steep mountainous  
44 catchments (Chen et al., 2018; Milliman and Kao, 2005). Warm sea-surface temperatures and reduced polar ice volumes  
45 under ~~past~~ greenhouse climates ~~likely amplified~~would likely amplify monsoon variability and produced frequent and intense  
46 tropical cyclones ~~that were considerably more intense and frequent than at present~~ (Fedorov et al., 2013). These conditions  
47 of elevated humidity and precipitation would have promoted not only enhanced chemical weathering of silicate rocks, but  
48 also greater terrestrial biomass production.

49 Land-to-sea export of terrestrial organic material from vegetation, soil, and rock is enhanced under high precipitation  
50 regimes, with steep mountain rivers efficiently transporting this material for burial in adjacent ocean basins (Milliman et al.,  
51 2017; Hilton et al., 2011). The global terrestrial carbon pool accounts for ~7.5% of the Earth's total carbon stock, excluding  
52 lithospheric carbon, and is more than five times larger than the atmospheric carbon pool (Canadell et al., 2021). As a result,  
53 even modest changes in the terrestrial carbon storage can significantly alter atmospheric CO<sub>2</sub> concentrations (Houghton,  
54 2003). In particular, physical erosion by water is widely recognized as a dominant control of land-atmosphere carbon  
55 exchange (Hilton and West, 2020; Van Oost et al., 2012). Elevated sediment discharge to the oceans would facilitate the  
56 export and burial of terrestrial organic carbon (Galy et al., 2007; Hilton et al., 2011; Liu et al., 2013; Aumont et al., 2001;  
57 Dagg et al., 2004; Jin et al., 2023), and also deliver bioessential nutrients that stimulate marine productivity (Hoshiba and  
58 Yamanaka, 2013; Krumins et al., 2013; Dürr et al., 2011; Beusen et al., 2016). However, the role of fluvial nutrient export in  
59 fuelling marine primary productivity is generally thought to be limited to coastal regions (Froelich, 1988; Stepanauskas et  
60 al., 2002; Dagg et al., 2004). This oversimplification in ocean biogeochemical models leads to a poorly constrained link  
61 between terrestrial nutrient supply, open-ocean productivity, and deep-sea carbon burial.

62 This research aims to address these knowledge gaps by disentangling the different mechanisms through which carbon is  
 63 sequestered as a result of low-latitude arc-continent collisions (Figure 1). A clearer understanding of these processes will  
 64 provide stronger constraints on both reconstructed and predictive carbon budget models. The study area focuses on the  
 65 northern South China Sea (SCS) region, specifically late Miocene to early Pleistocene (~6.3–2 Ma) strata of the Taiwan  
 66 Western Foreland Basin (TWFB, i.e., paleo-Taiwan Strait; Figure 2) and time-equivalent sediment core records obtained  
 67 from the Ocean Drilling Program (ODP Sites 1146 and 1148; Figure 2). Since its emergence in the early Pliocene, Taiwan  
 68 has been characterized by exceptionally high denudation rates and rapidly became the dominant sediment source to the  
 69 adjacent TWFB, overwhelming contributions from southeast Eurasia (Hsieh et al., 2023b). Hyperpycnal flows triggered by  
 70 intense precipitation transported Taiwan-derived sediments over 1000 km into the SCS, leaving a distinct signature in deep-  
 71 sea deposits (Hsieh et al., 2024; Liu et al., 2012). Strata of the TWFB capture the evolution of the Taiwan Orogen (Lin and  
 72 Watts, 2002), and thus provide insight into how changes in weathering and erosion processes modulated carbon burial in the  
 73 SCS sediments across successive orogenesis stages.



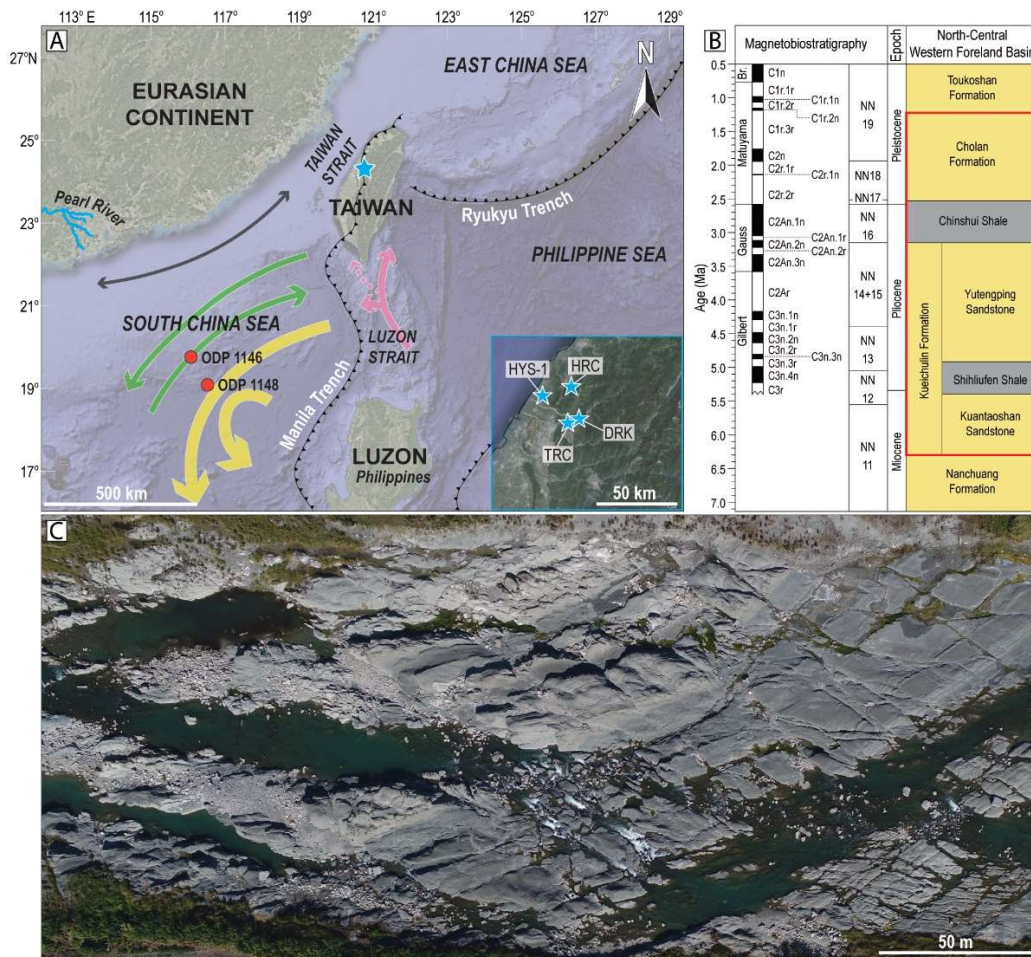
74  
 75 **Figure 1:Conceptual model of geologic carbon (C) sources and sinks, modified from (Berner, 2003).** This research focuses on two  
 76 main pathways of carbon sequestration often associated with arc-continent collisions, highlighted in blue: (1) direct burial of  
 77 terrestrial organic matter, and (2) nutrient-fuelled marine productivity followed by the burial of marine organic matter. These  
 78 processes play a crucial role in the long-term carbon cycle and the regulation of atmospheric CO<sub>2</sub>.

## 79 2 Study area

80 The base of the TWFB stratigraphic fill is composed of the Kueichulin Formation (~~Fm; late Miocene–early Pliocene~~), a  
 81 sandstone-dominated unit deposited between the late Miocene–early Pliocene in shallow-marine and deltaic environments  
 82 under the influence of wave and tidal processes, and composed of three members (from base to top): the Kuantaoshan  
 83 Sandstone, Shihliufen Shale, and Yutengping Sandstone (Figure 2; Castelltort et al., 2011; Nagel et al., 2013; Hsieh et al.,  
 84 2025). Overlying the Kueichulin Fm is the Chinshui Shale (late Pliocene), a mudstone-rich succession deposited

85 in the late Pliocene with uncommon wavy-laminated sandstone interbeds that accumulated in an offshore setting during a  
 86 phase of maximum flooding and enhanced subsidence in the TWFB (Castelltort et al., 2011; Nagel et al., 2013; Pan et al.,  
 87 2015). The Chinshui Shale is overlain by the Cholan Fm—Formation during the (early Pleistocene), which consists of  
 88 heterolithic sediments deposited in shallow-marine environments influenced by waves, rivers, and tides (Covey, 1986; Nagel  
 89 et al., 2013; Pan et al., 2015; Vaucher et al., 2023a).

90 The targeted time interval between (~6.27–1.95 Ma) was targeted because it spans the initiation of Eurasian–Philippine plate  
 91 collision through the Taiwan’s emergence and uplift of Taiwan by the ongoing Eurasian–Philippine plate collision. It also  
 92 includes the Pliocene (5.33–2.58 Ma), which may be the most recent time in Earth’s history when atmospheric CO<sub>2</sub> last  
 93 reached or exceeded present-day concentrations (>400 ppm; Tierney et al., 2019), and the subsequent transition toward  
 94 Pleistocene icehouse conditions. Additionally, since tectonic configurations, insolation, and major floral and faunal  
 95 assemblages have remained broadly unchanged since the mid-Pliocene (Dowsett, 2007; Robinson et al., 2008), this period  
 96 also provides a critical Earth system analogue for evaluating future climate hazards (e.g., Burke et al., 2018), including sea-  
 97 level rise and extreme weather events.



99 **Figure 2:A) Map of the study area showing the locations of the Late Miocene–Early Pleistocene records from Ocean Drilling**  
100 **Program (ODP) sediment cores (orange circles) in the South China Sea, and the outcrop of the Kueichulin Fmoutcrop locations**  
101 **from the Taiwan Western Foreland Basin (TWFB, blue stars). The inset map outlined in blue show the locations of the borehole**  
102 **(HYS-1) and outcrop locations (DRK = Da'an River, Kueichulin Formation; TRC = Tachia River, Chinshui Shale; HRC =**  
103 **Houlong River, Cholan Formation) of the TWFB strata used in this study. Modern-day circulation in the SCS is shown in arrows:**  
104 **black = alongshore surface current, red green = surface- and intermediate- water currents, green = intermediate-water current,**  
105 **yellow = deep- and bottom-water current, pink = Kuroshio current, pink (dashed) = Taiwan warm current (modified from Hu et**  
106 **al. (2010); Liu et al. (2010a); Liu et al. (2016); Yin et al. (2023)). B) Chronostratigraphy of the TWFB is modified after Chen**  
107 **(2016), Hsieh et al. (2023a), and Teng et al. (1991). The red box highlights the targeted study section. Yellow denotes sandstone-**  
108 **dominated strata, and grey indicates mudstone-dominated strata. C) Outcrop photo of the Chinshui Shale at Tachia River (this**  
109 **study).**

## 110 3 Methodology

### 111 3.1 Data acquisition and analysis

112 A total of 553 samples were collected from outcrops of the TWFB exposed along rivers in southwestern Taiwan, including  
113 272 collected from the Kueichulin Formation by Dashtgard et al. (2021) and Hsieh et al. (2023b) along the Da'an River  
114 (Figure 2A). This was combined with new data from the Chinshui Shale (n=90; Tachia River) and the Cholan FmFormation  
115 (n=191; Houlong River) (Figure 2A). Data between 4.13–3.15 Ma are not available as no outcrop sections were accessible.  
116 Gamma-ray data were obtained from the HYS-1 borehole drilled through the TWFB. Age-equivalent material was also  
117 obtained from deep-sea sediment cores ODP Site 1146 (19°27.40'N, 116°16.37'E, 2092 m water depth, 179.8–343.1 m core  
118 depth; Holbourn et al., 2005; Holbourn et al., 2007) and Site 1148 (18°50.169'N, 116°33.939'E, 3294 m water depth, 118.9–  
119 206 m core depth; Tian et al., 2008; Cheng et al., 2004), archived in international core repositories. Sampling resolution  
120 averaged ~1.4 m vertically through the TWFB stratigraphic sections, and ~0.65 m and ~0.35 m through the ODP Sites 1146  
121 and 1148 cores, respectively.

122 Samples from the Chinshui Shale and ODP sites were analysed for organic geochemistry and paleomagnetism. For the  
123 Chinshui Shale, total organic carbon (TOC) and total nitrogen (TN) concentrations were determined from pulverized rock  
124 samples in the Department of Geosciences at National Taiwan University (NTU) using an elemental analyser (Elementar  
125 TOC analyser soli TOC® cube; Lin et al., 2025). Total carbon (TC) and TN abundances for ODP samples were determined  
126 with a CHNS Elemental Analyser (Thermo Finnigan Flash EA 1112) at the Institute of Earth Sciences (ISTE) at the  
127 University of Lausanne in Switzerland on oven-dried sieved and crushed sediment samples. The samples were heated to  
128 900°C, after which the combustion products were extracted into a chromatographic column where they were converted into  
129 simpler components: CO<sub>2</sub> and N<sub>2</sub>. These components were then measured by a thermal conductivity detector, and the results  
130 were expressed as a weight percentage. Analytical precision and accuracy were determined by replicate analyses and by  
131 comparison with an organic analytical standard composed of purified L-cysteine, achieving a precision of better than 0.3%  
132 (REFS). Organic matter (OM) analyses of ODP core samples were performed on whole-rock powdered samples using a  
133 Rock-Eval 6 at the ISTE following the method described by Espitalie et al. (1985) and Behar et al. (2001). Measurements  
134 were calibrated using the IFP 160000 standard. Rock-Eval pyrolysis provides parameters such as hydrogen index (HI, mg

135 HC g<sup>-1</sup> TOC, HC = hydrocarbons), oxygen index (OI, mg CO<sub>2</sub> g<sup>-1</sup> TOC), *T<sub>max</sub>* (°C), and the TOC (wt.%). HI, OI and *T<sub>max</sub>* values, which give an overall measure of the type and maturation of the organic matter (e.g., Espitalie et al., 1985), can't be interpreted for TOC < 0.2 wt.% and *S<sub>2</sub>* values ≥ 0.2 mg HC g<sup>-1</sup>. Total organic carbon accumulation rates (mg cm<sup>-2</sup> kyr<sup>-1</sup>) for the ODP sites were calculated by multiplying mass-accumulation rates (MAR) derived from literature and TOC.

139 Organic carbon isotopic compositions ( $\delta^{13}\text{C}_{\text{org}}$ , ‰ relative to Vienna Pee Dee Belemnite) were measured by flash  
140 combustion on an elemental analyser (EA) coupled to an isotope-ratio mass spectrometer (IRMS) from pulverized,  
141 decarbonated (10% HCl treatment) whole-rock samples. Samples from ODP sites were analysed at the Institute of Earth  
142 Surface Dynamics, University of Lausanne, using a Thermo EA IsoLink CN connected to a Delta V Plus isotope ratio mass  
143 spectrometer (Thermo Fisher Scientific, Bremen), both operated under continuous helium flow. The samples and standards  
144 are weighed in tin capsules and combusted at 1020°C with oxygen pulse in a quartz reactor filled with chromium oxide  
145 (Cr<sub>2</sub>O<sub>3</sub>) and below with silvered cobaltous-cobaltic oxide. The combustion produced gases (CO<sub>2</sub>, N<sub>2</sub>, NO<sub>x</sub> and H<sub>2</sub>O) are  
146 carried by the He-flow to a second reactor filled with elemental copper and copper oxide wires kept at 640°C to remove  
147 excess oxygen and reduce non-stoichiometric nitrous products to N<sub>2</sub>. The gases are then carried through a water trap filled  
148 with magnesium perchlorate (Mg(ClO<sub>4</sub>)). The dried N<sub>2</sub> and CO<sub>2</sub> gases are separated with a gas chromatograph column at 70  
149 °C and then carried to the mass spectrometer. The measured  $\delta^{13}\text{C}$  values are calibrated and normalized using international  
150 reference materials and in-house standards Spangenberg, 2016. Samples from the Chinshui Shale were analysed at the Stable  
151 Isotope Laboratory at National Taiwan University using a Flash EA (Thermo Fisher Scientific) coupled to a Delta V  
152 Advantage (Thermo Fisher Scientific). The  $\delta^{13}\text{C}$  values are calibrated using an international reference material, IAEA-CH-3.  
153 The reproducibility and accuracy are better than ±0.1‰.

154 Thirty-three oriented palaeomagnetic core specimens (25-mm diameter) were collected at ~3.5 m intervals from  
155 unweathered, mud-rich beds [from the Chinshui Shale](#), then prepared and analysed at Academia Sinica in Taiwan following  
156 the methodology described in Horng (2014). Cores were cut into 2-cm samples, and bulk magnetic susceptibility measured  
157 using a Bartington Instruments MS2B magnetic susceptibility meter. Mass-specific magnetic susceptibility ( $\chi$ ) was then  
158 derived by normalising bulk magnetic susceptibility to sample mass.

159 Existing data for the ODP sites 1146 and 1148 were also compiled from literature, including clastic MAR (Site 1146 from  
160 Wan et al., 2010a, Site 1148 from Wang et al., 2000a), magnetic susceptibility (1146 from Wang et al., 2005a, 1148 from  
161 Wang et al., 2000a), hematite/goethite ratios (Hm/Gt) derived from spectral reflectance band ratios at 565/435 nm (1146  
162 from Wang et al., 2000b, 1148 from Clift, 2006), continuous gamma-ray logs (1146 from Wang et al., 2000b, 1148 from  
163 Wang et al., 2000a), and titanium/calcium ratios (Ti/Ca; 1146 from Wan et al., 2010a, 1148 from Hoang et al., 2010). [MAR](#),  
164 [m](#)[Magnetic susceptibility](#), and Ti/Ca serve as proxies for physical erosion, recording variations in terrigenous sediment flux  
165 linked to summer monsoon precipitation. Intensified precipitation enhances basin sediment accumulation rates (Clift et al.,  
166 2014), and typically increases the magnetic susceptibility of marine sediment via enhanced runoff and terrestrial input (Clift  
167 et al., 2002; Kissel et al., 2017; Tian et al., 2005). In the SCS, magnetic susceptibility also serves as a sediment provenance  
168 indicator. [Along the Taiwan Strait](#), [S](#)ediment sourced from western Taiwan yields  $\chi$  values that range from 0.9 ± 0.3 to 1.8

169  $\pm 0.5 \times 10^{-7} \text{ m}^3 \text{ kg}^{-1}$ , much lower than those sourced from the South China Block ( $4.0 \pm 1.3 \times 10^{-7} \text{ m}^3 \text{ kg}^{-1}$ ), indicating a  
 170 relative depletion of magnetic minerals in Taiwan-sourced material (Horng and Huh, 2011). Titanium, associated with heavy  
 171 mineral deposition, and calcium, linked to pelagic biogenic carbonate accumulation, yield Ti/Ca values that increase with  
 172 enhanced monsoon-driven sediment export (Clift et al., 2014). Gamma-ray intensities broadly track changes in lithology  
 173 (Green and Fearon, 1940; Schlumberger, 1989), where values  $< 75$  American Petroleum Institute (API) typically mark  
 174 sandstone-rich intervals,  $> 105$  API mudstone-rich intervals, and intermediate values reflect mixed lithologies. Increased  
 175 sediment export, particularly of coarser grains, may be expressed as lower API values.

176 Sedimentary TOC content provides a measure of organic carbon accumulation through time. Terrestrial and marine sources  
 177 can also be differentiated by their  $\delta^{13}\text{C}_{\text{org}}$  values (Dashtgard et al., 2021; Hilton et al., 2010; Chmura and Aharon, 1995;  
 178 Peterson and Fry, 1987; Martiny et al., 2013). Marine organic matter (e.g., plankton, particulate and dissolved organic  
 179 matter) typically have more enriched values than terrestrial inputs (e.g., C3 and C4 plants, and soil and lithogenic organic  
 180 carbon) (Table 1). Marine-derived organic matter mainly accumulates on the seafloor under fair-weather conditions, while  
 181 terrestrial input increases under intervals of increased precipitation and erosion (Hsieh et al., 2023b; Dashtgard et al., 2021).

182 **Table 1: Typical values for marine- and terrestrially sourced  $\delta^{13}\text{C}_{\text{org}}$  and C/N (compiled by Dashtgard et al., 2021). Numbers in**  
 183 **brackets represent sample count. OM = organic material.**

	Organic Material	$\delta^{13}\text{C}_{\text{org}} (\text{\textperthousand})$	C/N
Marine	Particulate OM	$-22.5 \pm 1.7$ (53)	$6.2 \pm 1.0$
	Plankton	$-20.4 \pm 1.4$ (184)	-
	Dissolved OM	$-22.5 \pm 0.8$ (23)	-
Terrestrial	All pelagic marine organic matter - equally weighted	$-21.8 \pm 1.7$	$6.2 \pm 1.0$
	High- $^{13}\text{C}$ plants (C4)	$-13.2 \pm 1.9$ (89)	$83.3 \pm 54$ (6)
	Low- $^{13}\text{C}$ plants (C3)	$-27.4 \pm 1.9$ (161)	$52 \pm 14.8$ (55)
	Soil	$-25.9 \pm 1.2$ (11)	$17.1 \pm 7.3$ (22)

184

185 Hematite-to-goethite (Hm/Gt) ratios are widely applied as indicator of monsoon precipitation (Clift, 2006; Liu et al., 2007;  
 186 Zhang et al., 2009). Hematite typically forms through iron oxidation under arid climates [or seasonal climates with dry](#)  
 187 [seasons](#), whereas goethite preferentially develops under humid climates (e.g., Kämpf and Schwertmann, 1983; Maher, 1986).  
 188 In the northern SCS, however, Clift et al. (2014) documented a positive relationship between elevated Hm/Gt values and  
 189 intensified East Asian Summer Monsoon (EASM) rainfall and seasonality. Beyond climate, hematite also reflects sediment  
 190 provenance: sediment derived from Taiwan is notably depleted in hematite and enriched in pyrrhotite (Horng and Huh,

191 2011). Locally estimated scatterplot smoothing (LOESS) is applied to all data to reveal trends through the studied time  
192 interval (Cleveland et al., 1992).

193 **3.2 Age models**

194 The chronostratigraphic framework for the Kueichulin FormationFm, Chinshui Shale, and andCholan FormationFm of the  
195 TWFB was established by astronomically tuning the gamma-ray records to the  $\delta^{18}\text{O}$  record of Wilkens et al. (2017) (Hsieh et  
196 al., 2023a; Vaucher et al., 2023b). However, the boundary between the top of the Kueichulin FormationFm and the base of  
197 the Chinshui Shale is not well-established. Therefore, a magnetobiostratigraphic age model was developed from nannofossil  
198 zones and magnetic reversals identified in oriented outcrop core samples from the Chinshui Shale outcrop using the  
199 methodology described in Horng (2014) to ground-truth the existing framework. The remanent magnetic intensity, and  
200 declination and inclination of oriented core samples were measured using a JR-6A spinner magnetometer (AGICO). To  
201 determine the stable remanent magnetization and polarity (i.e., normal or reversed) of each sample, unstable secondary  
202 magnetization was removed by thermally demagnetizing the samples stepwise from 25 to 600°C. The characteristic  
203 remanent magnetization (ChRM) declination and inclination of thermally demagnetized samples were calculated using  
204 principal component analysis with a minimum of three demagnetization steps in the PuffinPlot software (Lurcock and  
205 Wilson, 2012) to determine the polarity of each sample. Thermal demagnetization diagrams for the Chinshui Shale samples  
206 showing the stable remanent magnetic declinations and inclinations after principal component analysis are presented in  
207 Figure S1 in Supporting Information.

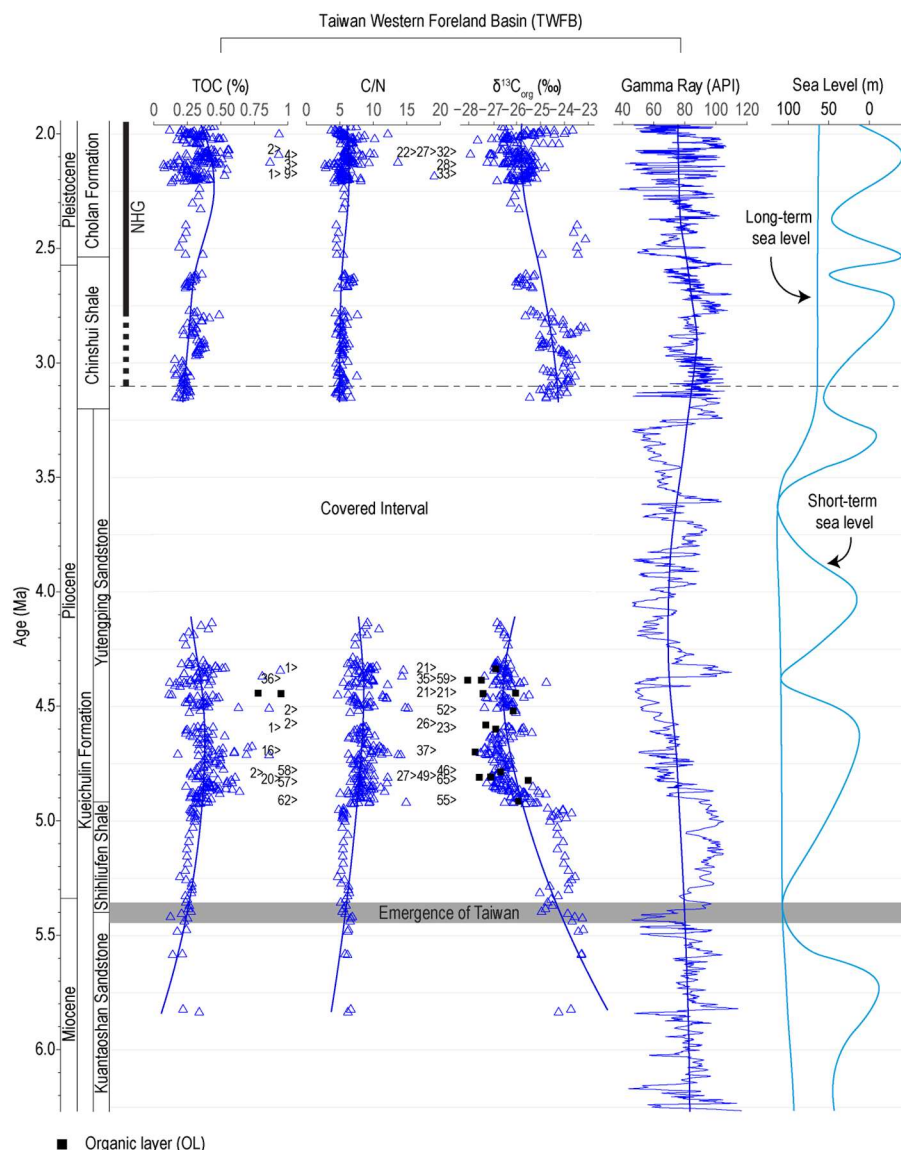
208 Index nannofossils and corresponding biozonations identified by Shea and Huang (2003) for the Chinshui Shale were used to  
209 constrain paleomagnetic polarities. The resulting age model was then correlated to an orbitally tuned, benthic foraminiferal,  
210 stable oxygen isotope ( $\delta^{18}\text{O}$ ) record from the equatorial Atlantic Ocean (Wilkens et al., 2017), which is tied to physical  
211 sedimentary properties independent of ice volume, and has a robust timescale. Variations in both parameters are assumed to  
212 be causally linked and temporally in-phase.

213 The age model for ODP Site 1146 (Wan et al., 2010a) was constructed by linear interpolation between  
214 magnetobiostratigraphic age control points established by Wang et al. (2000b). Stratigraphic ages from ODP Site 1148 (Clift,  
215 2006) are constrained using biostratigraphic ages of benthic foraminifera (Wang et al., 2000a).

216 **4 Results**

217 Data collected from the Chinshui Shale ( $n = 90$ ) for this study have average TOC values ( $0.3 \pm 0.1\%$ ) comparable to the  
218 those of the Shihliufen Shale ( $0.3 \pm 0.03\%$ ,  $n = 31$ ), but are higher than the basal Kuantaoshan Sandstone ( $0.2 \pm 0.1\%$ ,  $n = 9$ ),  
219 and lower than the Yutengping Sandstone ( $0.4 \pm 0.1\%$ ,  $n = 216$ ) and the Cholan FormationFm ( $0.4 \pm 0.7\%$ ,  $n = 191$ ; Figure  
220 3). C/N and  $\delta^{13}\text{C}_{\text{org}}$  values of the Chinshui Shale ( $5.2 \pm 0.7$  and  $-24.5 \pm 0.7\text{‰}$ , respectively) indicate stable accumulation of  
221 marine organic content, similar to the Shihliufen Shale ( $5.3 \pm 0.4$  and  $-24.2 \pm 0.4\text{‰}$ ) in contrast to the Kuantaoshan

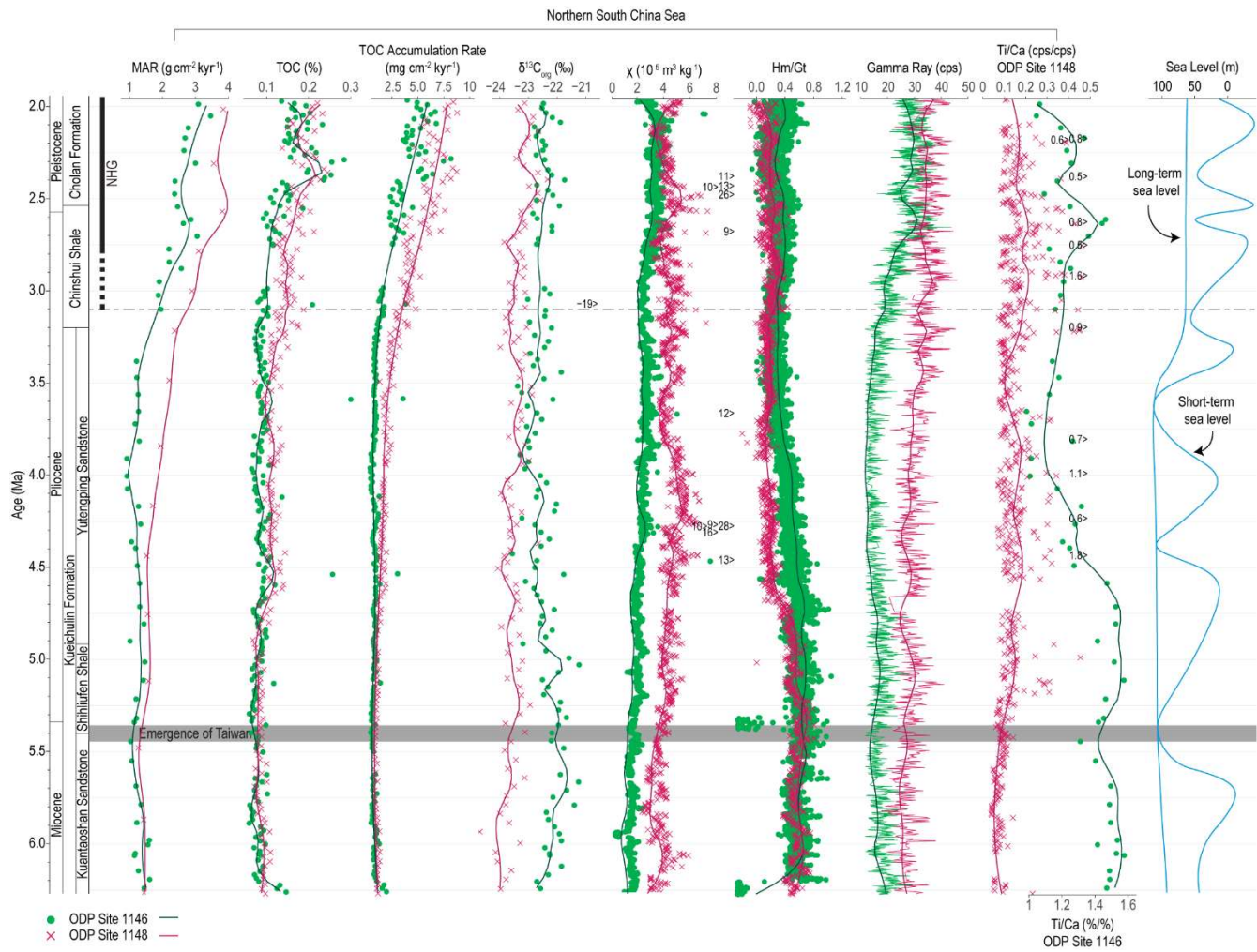
222 Sandstone ( $6.1 \pm 0.3$ ,  $-23.4 \pm 0.3\text{‰}$ ), Yutengping Sandstone ( $8.5 \pm 1.8$ ,  $-26.5 \pm 0.5\text{‰}$ ), as well as the overlying Cholan  
 223 Formation  
 224 organic matter is also stable through the Shihliufen Shale and the Chinshui shale, with greater variability between  $\sim 4.9\text{--}4$  Ma  
 225 (Yutengping Sandstone), and after  $\sim 2.3$  Ma (Cholan Formation; Figure 3).



226  
 227 **Figure 3: Compilation of total organic carbon (TOC), C/N,  $\delta^{13}\text{C}_{\text{org}}$ , and gamma ray data for the Taiwan Western Foreland Basin**  
 228 (**TWFB**), including the Kueichulin Formation  
 229 (**Formation**  
 230 (Dashtgard et al., 2021; Hsieh et al., 2023b; Hsieh et al., 2023a), the Chinshui  
 231 Shale (this study and gamma-ray from Vaucher et al. (2023b)), and the Cholan Formation  
 232 (this study and gamma-ray from Vaucher et al. (2023b)). Sea-level curves are from Haq and Ogg (2024). “>” indicates data that plot outside of the diagram. The  
 233 solid lines represent curves fitted using locally estimated scatterplot smoothing (LOESS). TOC, C/N, and  $\delta^{13}\text{C}_{\text{org}}$  trends reflect  
 234 organic carbon sources, and show that marine organic matter content is high in the Kuantaoshan Sandstone, Shihliufen Shale, and  
 Chinshui Shale, contrasting with increased terrestrial input in the Yutengping Sandstone and Cholan Formation. Gamma-ray  
 data indicate lithological variability, and correlate with sea-level changes.

235 At ODP Site 1146 (Figure 4), MAR (n=59) and TOC (n = 225) values remain relatively stable until ~3.3 Ma (averaging 1.2  
236  $\pm 0.2 \text{ g cm}^{-2} \text{ kyr}^{-1}$  and  $0.08 \pm 0.03\%$ , respectively), after which both increase, with a maximum MAR of  $3.5 \text{ cm}^{-2} \text{ kyr}^{-1}$ , and  
237 maximum TOC of 0.3%, accompanied by greater TOC variability. This is reflected in the TOC accumulation rate (n = 225),  
238 which shows increasing trends also since ~3.3 Ma, from an average of  $9.6 \pm 3.7 \times 10^{-4}$  to  $3.7 \pm 1.8 \times 10^{-3} \text{ mg cm}^{-2} \text{ kyr}^{-1}$ .  
239  $\delta^{13}\text{C}_{\text{org}}$  (n = 113) show a gradual decrease from ~5.7–4 Ma from an average of  $-21.8 \pm 0.4$  to  $-22.2 \pm 0.6\text{\textperthousand}$ , then stabilises.  
240 Magnetic susceptibility (n = 2747) increases through the record from an average of  $\sim 1.6 \pm 0.4$  to  $2.5 \pm 1 \times 10^{-5} \text{ m}^3 \text{ kg}^{-1}$  from  
241 5–3 Ma, with accelerated increase after ~3 Ma. Hm/Gt ratios (n = 8196) decrease gradually from ~4.75–3 Ma (from an  
242 average of  $0.56 \pm 0.3$  to  $0.35 \pm 0.1$ , before showing greater amplitude variability. Gamma-ray values (n = 2551) remain  
243 relatively stable ( $16.2 \pm 3.3$  API) until ~3.2 Ma with when both values and amplitudes rise ( $26.7 \pm 5.7$  API). The Ti/Ca  
244 record (%%, n = 53) shows an overall decreasing trend from ~4.6 Ma–3.5 Ma from an average of  $1.5 \pm 0.07$  to  $1.2 \pm 0.1$ .  
245 At ODP Site 1148 (Figure 4), MAR values (n = 15) remain stable with a slight increase at ~5.5 Ma from an average of  $1.4 \pm$   
246  $0.009$  to  $1.6 \pm 0.2 \text{ g cm}^{-2} \text{ kyr}^{-1}$ , followed by a sharper increase near ~3.5 Ma to a maximum of  $3.5 \text{ g cm}^{-2} \text{ kyr}^{-1}$ . TOC values (n  
247 = 220), as well as TOC accumulation rates (n = 220), are stable from ~6.27–4.7 Ma (averaging  $0.08 \pm 0.01\%$  and  $1.1 \pm 0.2 \times$   
248  $10^{-3} \text{ mg cm}^{-2} \text{ kyr}^{-1}$ , respectively. Both TOC and TOC accumulation rates increase from ~4.7–4.5 Ma to  $0.11 \pm 0.01\%$  and  $1.9 \pm$   
249  $0.3 \times 10^{-3} \text{ mg cm}^{-2} \text{ kyr}^{-1}$ , then stabilize until ~3.5 Ma, and then increased again (exceeding 0.2% and  $5 \times 10^{-3} \text{ mg cm}^{-2} \text{ kyr}^{-1}$ ,  
250 respectively) with greater amplitude. MAR, TOC, and TOC accumulation rates also exceed values measured from Site 1146  
251 since ~4.7 Ma by 20–60%.  $\delta^{13}\text{C}_{\text{org}}$  (n = 110) is broadly stable, increasing near ~2.75 Ma from an average of  $-23.2 \pm 0.3$  to  $-22.8 \pm 0.4\text{\textperthousand}$ . Magnetic susceptibility values (n = 1249) show a gradual increase from ~5.4–4.3 Ma from an average of  $3.6 \pm$   
252  $0.6$  to  $4.9 \pm 0.8 \times 10^{-5} \text{ m}^3 \text{ kg}^{-1}$ , then a decrease until ~3.5 Ma to an average of  $4.6 \pm 1.2 \times 10^{-5} \text{ m}^3 \text{ kg}^{-1}$ . The values remain low  
253 after ~3.5 Ma, with amplitudes deceasing after ~2.75 Ma. Hm/Gt (n = 1678) declines from ~5.4–4.6 Ma from an average of  
254  $0.61 \pm 0.08$  to  $0.2 \pm 0.06$ , then stabilizes and slightly increases from ~3.2–2.9 Ma. Gamma-ray values (n = 1249) are high  
255 from ~5.4–4.9 Ma, averaging  $29.5 \pm 3.8$  API, then decrease and stabilize before rising again after ~3.5 Ma to an average of  
256  $35 \pm 4.2$  API. The Ti/Ca ratios (cps/cps, n = 646) increase overall from ~5.4 Ma, from an average of  $0.07 \pm 0.03$  to  $0.16 \pm$   
257 0.1, with increasing amplitude variability.

|259



260  
261 **Figure 4: Compilation of sediment core data from ODP Sites 1146 and 1148 in the northern South China Sea, including mass**  
262 **accumulation rate (MAR; Wan et al., 2010a; Wang et al., 2000a), TOC and  $\delta^{13}\text{C}_{\text{org}}$  (this study), mass-specific magnetic**  
263 **susceptibility ( $\chi$ ; Wang et al., 2005a; Wang et al., 2000a), hematite/goethite (Hm/Gt; Wang et al., 2000b; Clift, 2006), gamma ray**  
264 **(Wang et al., 2000b, a), and Ti/Ca (Wan et al., 2010a; Hoang et al., 2010). Sea-level curves are from Haq and Ogg (2024). “>”**  
265 **indicates data that plot outside of the diagram. The solid lines represent curves fitted using locally estimated scatterplot smoothing**  
266 **(LOESS). The figure illustrates the contrasting sedimentary and geochemical responses between the two ODP sites, driven by**  
267 **tectonic uplift, climate variability, and changes in ocean circulation.**

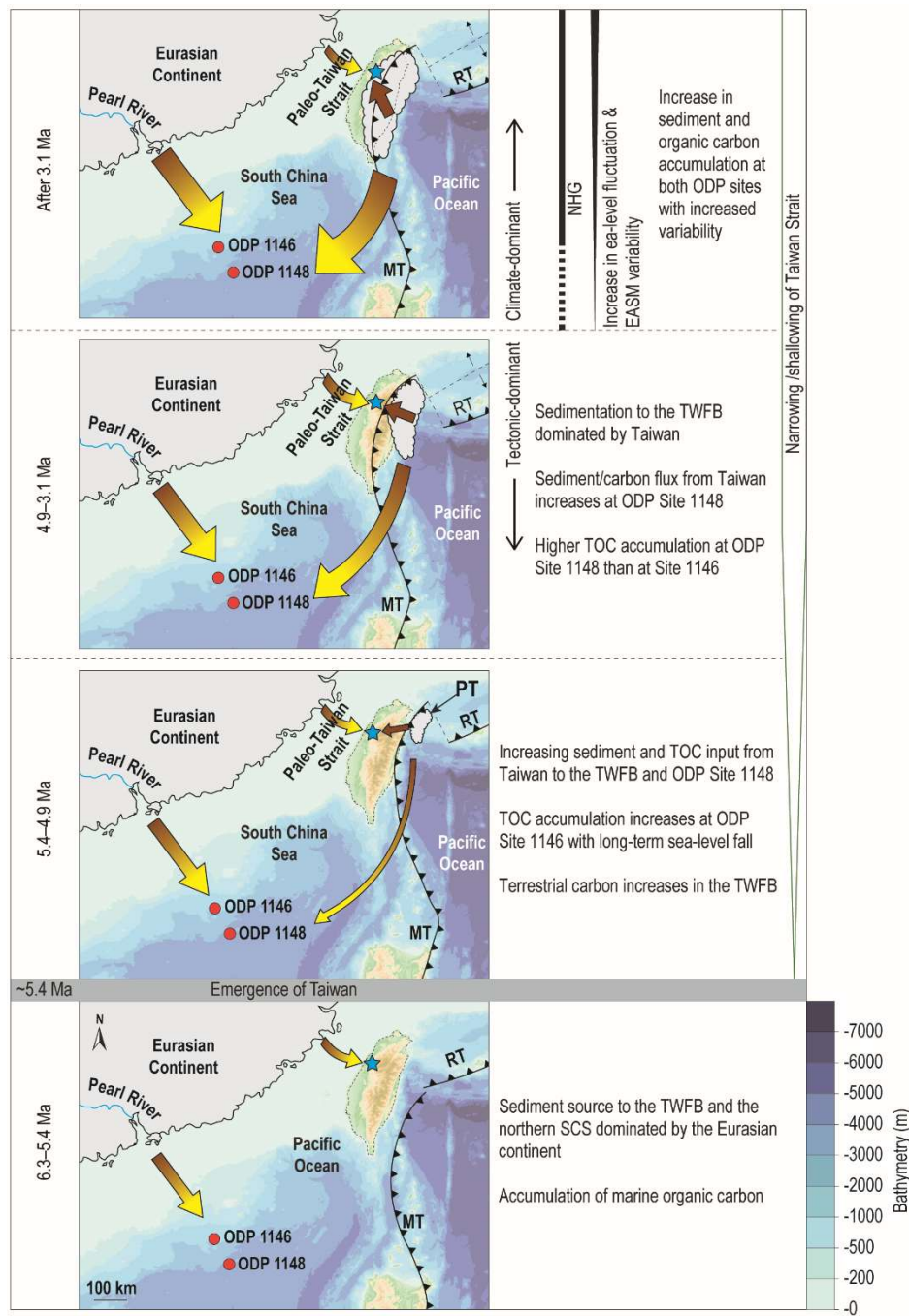
268 **5 Discussion**

269 **5.1 Spatial variability in sediment provenance and distribution in the northern South China Sea**

270 Provenance exerts a first-order control on sedimentary records in the SCS, owing to the region’s complex geology and active  
271 tectonism, which channels sediment contributions from multiple major rivers (e.g., Clift et al., 2014; Clift et al., 2022; Horng  
272 and Huh, 2011; Kissel et al., 2016, 2017; Liu et al., 2009c; Liu et al., 2007; Liu et al., 2010b; Liu et al., 2016; Wan et al.,

273 2010c; Milliman and Syvitski, 1992). During most of the Neogene, the Pearl River supplied the dominant sediment flux to  
274 the northern SCS (Clift et al., 2002; Li et al., 2003). The emergence of the Taiwan orogen in the early Pliocene  
275 fundamentally reorganised this system: by ~5.4 Ma, and especially after ~4.9 Ma, Taiwan had become a major sediment  
276 source to the adjacent TWFB and the wider SCS, as a result of rapid uplift and intense erosion and ~~southwestward~~<sup>south</sup>  
277 ~~westward~~ collision-zone migration (Figure 5; Liu et al., 2010b; Hsieh et al., 2023b; Hu et al., 2022). This change in sediment  
278 provenance is tectonically driven and underscores the need to disentangle tectonic from climatic signals in SCS sedimentary  
279 archives (Clift et al., 2014; Hsieh et al., 2024).

280 This diversity in sediment sources and mixing is reflected at ODP Sites 1146 and 1148, where the sediment records  
281 ~~divergediffer~~ despite their spatial proximity. MAR, magnetic susceptibility, Hm/Gt and gamma-ray records diverge between  
282 the two sites until ~3 Ma (Figure 4). At ODP Site 1146, located on the continental slope, sediments are primarily derived  
283 from Eurasia (Figure 5). At Site 1146, major element and clay mineral compositions point to a mixture of sources dominated  
284 by the Pearl River, with additional inputs from the Yangtze River, Taiwan, Luzon, and loess (Wan et al., 2007a; Liu et al.,  
285 2003; Hu et al., 2022). Pearl River sediment ~~discharge-deposition~~ is controlled by long-term sea-level changes and East  
286 Asian Monsoon variability (e.g., Liu et al., 2016; Clift, 2006), but its ~~delivery to the open basin~~<sup>transport</sup> is strongly  
287 constrained ~~by : the northward flowing Kuroshio Current and shallow Taiwan Strait, limit delivery to the open basin,~~  
288 ~~instead alongshore and surface- to intermediate-water currents that~~ funnelling most material along the continental shelf and  
289 slope ~~via alongshore currents~~ (Liu et al., 2010b; Liu et al., 2016; Wan et al., 2007a; Liu et al., 2009a).



290

291 **Figure 5: Summary of different controls on sediment and carbon accumulation over time in the Taiwan Western Foreland Basin** (blue star)  
292 and the ODP sites (pink-orange circles) in the northern South China Sea. The size of the arrows indicates relative  
293 proportions of sediment flux, and green-brown indicates accumulation of terrestrial organic carbon, while blue-yellow  
294 indicates marine organic carbon. The abbreviations MT = Manilla Trench, RT = Ryukyu Trench, and PT = proto-Taiwan. These  
295 differences in organic carbon source (i.e., terrestrial vs. marine) and carbon accumulation highlight the spatial heterogeneity in

296 sedimentary and geochemical records within the northern South China Sea, shaped by the interplay of tectonic and climatic  
297 processes. Bathymetric map from Gebco Compilation Group, 2025).

298 In contrast, ODP Site 1148, located on the continental rise, records a stronger Taiwanese imprint (i.e., less contribution from  
299 Eurasia; Figure 5). Prior to ~6.5 Ma, major element data suggest a mixture of Pearl River and Taiwan inputs, but since the  
300 onset of Taiwan orogenesis (~6.5 Ma), Taiwanese material has increasingly dominated (Hu et al., 2022). Isotopic ( $^{87}\text{Sr}/^{86}\text{Sr}$ ,  
301  $\varepsilon_{\text{Nd}}$ ) records, and clay mineralogy showing increasing illite with corresponding decreasing kaolinite near ~5 Ma clay mineral  
302 records corroborate Taiwan as the dominant sediment contributor to the northern SCS since its emergence after ~5.4 Ma  
303 (Bertaz et al., 2024; Boulay et al., 2005; Clift et al., 2014; Hsieh et al., 2023b). This conclusion is also supported by rare  
304 earth element studies that attribute up to 80% of slope sediments to the Taiwan orogen, and < 20% to the Pearl River (Shao  
305 et al., 2009; Shao et al., 2001). Erosion of modern and ancient Taiwan is primarily driven by tropical-cyclone precipitation  
306 (Dashtgard et al., 2021; Vaucher et al., 2021; Galewsky et al., 2006; Chen et al., 2010; Chien and Kuo, 2011; Janapati et al.,  
307 2019). Under warmer Pliocene climates (Fedorov et al., 2010; Yan et al., 2016) such storms were likely more frequent and  
308 intense (e.g., Yan et al., 2019), and especially if coinciding with EASM circulation, would have driven exceptionally high  
309 precipitation (Chen et al., 2010; Chien and Kuo, 2011; Kao and Milliman, 2008; Lee et al., 2015; Liu et al., 2008) and  
310 sediment export (Vaucher et al., 2023b). Sediment derived from Taiwan is subsequently redistributed into the northern SCS  
311 by downslope deep currents (Liu et al., 2010b; Liu et al., 2016; Hu et al., 2012; Liu et al., 2013). The emergence of Taiwan  
312 also reconfigured regional circulation, establishing a westward Kuroshio branch that delivered additional sediment from  
313 Taiwan and the Philippines (i.e., the Luzon Arc) into the northern basin (Liu et al., 2016).

314 The difference in sediment provenance and transport pathways between the continental slope and continental rise is reflected  
315 in the contrasting proxy trends observed at both ODP sites (Figure 4). At ODP Site 1146, the long-term increase in magnetic  
316 minerals since ~6.27 Ma reflects increased sediment input from Eurasia that is comparatively enriched in magnetic minerals  
317 than sediment from Taiwan (Horng and Huh, 2011; Hsieh et al., 2023b). Concurrently, low gamma-ray values and declining  
318 Ti/Ca until ~3 Ma also reflect increased delivery of sand-rich, clastic detritus, while the decreasing Hm/Gt suggests a  
319 progressive weakening of the EASM rainfall and seasonality. Together, these proxy signals are consistent with global trends  
320 of long-term cooling and falling global mean sea level during this interval (Wan et al., 2007b; Haq et al., 1987; Miller et al.,  
321 2020; Westerhold et al., 2020; Holbourn et al., 2021; Berends et al., 2021; Rohling et al., 2014; Jakob et al., 2020; Haq and  
322 Ogg, 2024), as well as with evidence of diminished chemical weathering and progressive weakening of the EASM system  
323 (Clift et al., 2014; Wan et al., 2006; Wan et al., 2010a; Wan et al., 2010b; Clift, 2025; Li et al., 2004; Wang et al., 2019).  
324 This interpretation is further supported by declining K/Al ratios observed at ODP Site 1146 between 5 and 3.8 Ma by Tian et  
325 al. (2011), which likewise indicate reduced chemical weathering and a shift towards long-term drying which began ~10 Ma  
326 in the region (Clift, 2025; Clift et al., 2014).

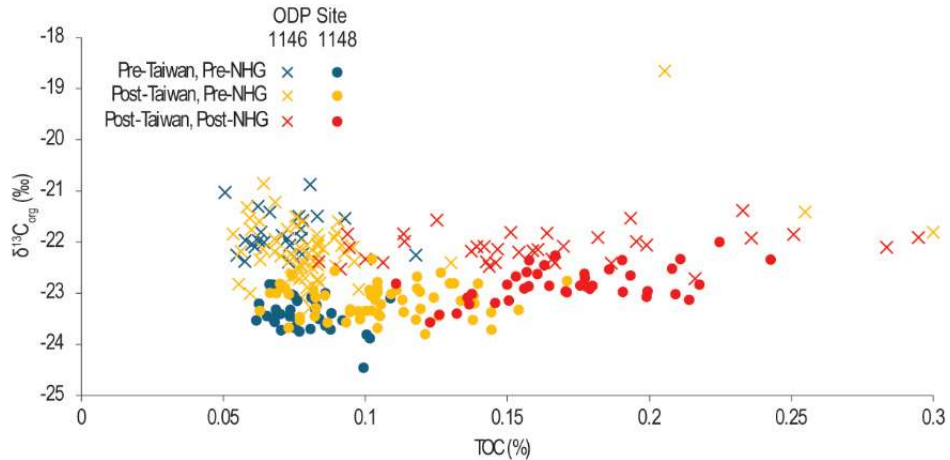
327 At ODP Site 1148, MAR increases near the onset of Taiwan's orogenesis (~5.4 Ma), reflecting corresponding to enhanced  
328 sediment export from rapid erosion of the emerging orogen. An increase in magnetic susceptibility is also observed ~5.4–4.3  
329 Ma (Figure 4), consistent with the erosion of passive-margin seafloor sediments enriched in magnetic minerals that was

330 uplifted during the early stages of Taiwan's orogenesis (Hsieh et al., 2023b). After ~4.3 Ma, magnetic susceptibility declines,  
331 coinciding with the deposition of the Yutengping Sandstone and increasing influx of sediment derived from the  
332 metasedimentary core of Taiwan, which is comparatively depleted in magnetic minerals (Hsieh et al., 2023b). Unlike Site  
333 1146, the Hm/Gt record at Site 1148 does not appear to track long-term ~~the~~ monsoon drying. Rather, the abrupt decrease in  
334 the Hm/Gt record at ~5.4 Ma is attributed to the influx of hematite-depleted sediment from Taiwan as it emerged from the  
335 Pacific Ocean. The dispersal of Taiwan-sourced sediment into the northern SCS was facilitated by deep-water currents and  
336 by the westward-flowing Kuroshio Branch, both of which developed following the formation of the Taiwan and Luzon  
337 straits during orogenesis. Changes in ocean circulation during the early to middle Pliocene are also captured by K/Al records,  
338 which show contrasting trends between intermediate water depths (e.g., Site 1146) and deep water settings (e.g., Site 1148),  
339 which is interpreted as reflecting shifts in sediment dispersal pathways to the northern SCS (Tian et al., 2011). The  
340 subsequent rise in Hm/Gt near ~3.2 Ma is attributed to the northward remobilization of Taiwan-sourced sediment following  
341 the formation of ~~the~~ Taiwan Warm Current (Figure 3; Hsieh et al., 2024). The gamma-ray record also tracks the orogenic  
342 evolution of Taiwan at ~~both ODP sites~~ ODP Site 1148 (Figure 4) and parallels observations from the TWFB (Figure 3):  
343 values are elevated during the deposition of mudstone-rich Shihliufen Shale, decrease during formation of sand-dominated  
344 Yutengping Sandstone and rise again with the deposition of mudstone-rich Chinshui Shale and Cholan Formation Fm. The  
345 increase in sediment export from Taiwan is also reflected in the Ti/Ca record, which increases after ~5.4 Ma, in response to  
346 intensified physical erosion and elevated terrestrial flux linked to the onset of Taiwan orogenesis.  
347 After ~3 Ma, the onset of Northern Hemisphere Glaciation (NHG) resulted in enhanced seasonality and an intensification of  
348 the EASM (Figure 5; Clift, 2025; Wan et al., 2006; Clift et al., 2014; Wan et al., 2007a; Wan et al., 2007b). Although global  
349 cooling characterized the late Plio-Pleistocene (Lisiecki and Raymo, 2005), sea-surface temperatures in the northwest Pacific  
350 remained sufficiently high (26.5–27.0°C) to sustain tropical cyclone activity (Tory and Frank, 2010). This combined  
351 influence of intensified EASM and frequent tropical-cyclone precipitation promoted elevated sediment production and large-  
352 scale export of fine-grained material enriched in TOC from river catchments into offshore depocenters. This is reflected in  
353 both sites by higher gamma-ray values, increased MAR, and rising Ti/Ca ratios (Figure 4). Enhanced seasonality is further  
354 expressed in the greater amplitude observed in gamma-ray, Hm/Gt, and Ti/Ca records.

## 355 **5.2 Influence of terrestrial sediment export vs. primary production on carbon burial**

356 Organic carbon buried in the SCS can be broadly divided into two components: (1) terrestrial organic matter derived from  
357 rock, soil, and terrestrial vegetation exported from adjacent landmasses by precipitation-driven erosion, and (2) marine  
358 organic matter produced by primary productivity and exported to the seafloor.  
359 At Site 1146, organic carbon accumulation, like bulk sediment accumulation, is primarily controlled by long-term global  
360 sea-level fall associated with the onset and intensification of NHG (Figure 5). Total organic carbon values are closely  
361 coupled with MAR, with increases in sediment flux consistently accompanied by higher TOC concentrations (Figure 4).  
362 Although  $\delta^{13}\text{C}_{\text{org}}$  values show a modest decline between ~5.7 and 4.5 Ma, which is consistent with episodic dilution by

363 terrestrial organic inputs, values remain within the marine range (Table 1). The gradual increase in terrestrial organic matter  
 364 at ODP Site 1146 is interpreted to reflect increased Eurasian clastic influx under conditions of long-term sea-level fall. The  
 365 cross-plot of  $\delta^{13}\text{C}_{\text{org}}$  and TOC also shows no distinct shift between organic matter delivered to Site 1146 before and after the  
 366 emergence of Taiwan. As sediment transported eastward from the Eurasian margin would have longer residence times in the  
 367 ocean, the dilution of land-derived organic material by marine organic material would increase, resulting in a more marine  
 368  $\delta^{13}\text{C}_{\text{org}}$  signature (Dashtgard et al., 2021) which supports the interpretation that organic material is derived mainly from  
 369 Eurasia via the Pearl River (Figure 6).



370  
 371 **Figure 6: Cross-plot of  $\delta^{13}\text{C}_{\text{org}}$  and TOC measured from ODP Sites 1146 and 1148. Values are grouped according to major tectonic  
 372 and climate changes: 1) pre-emergence of Taiwan and pre-Northern Hemisphere Glaciation, 2) post-emergence of Taiwan and  
 373 pre-Northern Hemisphere Glaciation, and 3) post-emergence of Taiwan and post-Northern Hemisphere Glaciation. Note the  
 374 distinct trends before and after Taiwan's emergence and Northern Hemisphere Glaciation. Site 1146 reflects Eurasian sediment  
 375 input with marine organic matter dominance, while Site 1148 highlights Taiwan's influence, with enhanced marine productivity  
 376 linked to nutrient export.**

377 In contrast, carbon burial at Site 1148 is primarily linked to the uplift and erosion of Taiwan and associated increase in  
 378 sediment and nutrient delivery to the marine environment (Figure 5). The onset of [orogenesis in Taiwan](#) [Taiwan's emergence](#)  
 379 at  $\sim 5.5$  Ma coincides with a marked rise in MAR, followed by an increase in TOC beginning near  $\sim 4.9$  Ma (Figure 4). This  
 380 pattern [indicates reflects](#) significant export of terrestrial sediment from the rapidly uplifting Taiwan orogen, a process further  
 381 amplified by the coupling between tropical cyclone and monsoon precipitation (Vaucher et al., 2023b). Notably, TOC  
 382 increases proportionally with MAR, implying that carbon burial was not diluted by high sediment flux but rather enhanced  
 383 by intensified sediment export [and/or better preserved by rapid burial](#), highlighting the role of Taiwan as a contributor of  
 384 organic carbon in the northern SCS. The influence of sedimentation from Taiwan on organic matter buried at Site 1148 is  
 385 also evident from the cross-plot between  $\delta^{13}\text{C}_{\text{org}}$  and TOC, which shows a distinct increase in TOC prior to and after the  
 386 emergence of Taiwan (Figure 6).

387 Taiwan's steep topography and active tectonics generate exceptionally high sediment yields to adjacent marine systems (Liu  
 388 et al., 2013; Dadson et al., 2003; Dadson et al., 2004). Turbidity currents, especially via submarine canyon systems (e.g., the

389 Gaoping Submarine Canyon in southern Taiwan), efficiently transport organic-rich sediment eroded from Taiwan to deep-  
390 sea environments approximately 260 km offshore into the northeastern Manila Trench (Liu et al., 2009b; Liu et al., 2016;  
391 Zheng et al., 2017; Yu et al., 2009; Nagel et al., 2018). Within the TWFB, this process is manifested as an abrupt increase in  
392 terrestrial organic matter and sand-rich deposition near ~4.9 Ma with the emplacement of the Yutengping Sandstone (Figure  
393 4). At Site 1148, TOC increases markedly in association with the emergence of Taiwan, and  $\delta^{13}\text{C}_{\text{org}}$  values remain stable  
394 above -25‰. While C<sub>4</sub> plants are characterized by high  $\delta^{13}\text{C}_{\text{org}}$  values (Table 1), and an expansion of C<sub>4</sub> plants in the South  
395 China region has been documented since 35 Ma (Li et al., 2023; Xue et al., 2024), the organic carbon at Site 1148 are  
396 interpreted to be of marine in origin as C<sub>3</sub> plants remain the dominant vegetation type in the study area (Luo et al., 2024; Still  
397 et al., 2003; Wang and Ma, 2016). Furthermore, sediment provenance markers (Section 5.1) indicate an influx of Taiwan-  
398 sourced material to Site 1148 after the emergence of Taiwan, and  $\delta^{13}\text{C}_{\text{org}}$  values in the TWFB reflect an increase in terrestrial  
399 organic matter. The presence of Taiwan-sourced material combined with high proportions of marine organic carbon at Site  
400 1148 suggests that terrestrial organic matter from Taiwan was largely confined to proximal coastal environments, and that  
401 enhanced carbon burial in deeper settings reflects processes beyond direct terrigenous input. Likewise, terrestrial organic  
402 matter contribution from the Pearl River into deeper-water depocenters is limited, as sediment is dispersed along the  
403 continental shelf by alongshore and shallow- to intermediate-water currents (Liu et al., 2010b; Liu et al., 2016; Wan et al.,  
404 2007a). During transport and sedimentation, degradation does not appear to significantly alter the isotopic composition of  
405 organic matter, since there is little fractionation between reactants and products. If post-depositional alteration were a  
406 dominant control,  $\delta^{13}\text{C}_{\text{org}}$  values should become progressively less negative with depth, as lighter isotopes are preferentially  
407 removed. However, the  $\delta^{13}\text{C}_{\text{org}}$  records from the two sites show distinct trends, suggesting that the influence of post-  
408 depositional isotopic fractionation is insignificant.

409 Taiwan's rapid denudation delivers large quantities of sediment and nutrients to the northern SCS, profoundly shaping basin  
410 productivity and carbon cycling. The export of bioessential nutrients stimulates intense coastal primary production, as  
411 reflected by modern chlorophyll-a and nitrogen distributions that peak along Taiwan's coast before rapidly declining  
412 offshore due to swift uptake (Kao et al., 2006; Ge et al., 2020; Huang et al., 2020). Episodic inputs from tropical cyclones,  
413 which contribute up to 80% of summer particulate organic carbon, further amplify productivity and promote lateral dispersal  
414 of sediments (Liu et al., 2013). Marine organic matter produced through enhanced coastal productivity could be redistributed  
415 by deep-water contour currents and mesoscale eddies, (Lüdmann et al., 2005; Zhang et al., 2014; Zhao et al., 2015; Hsieh et  
416 al., 2024), enabling its bypass into the deeper water depths and resulting in the marine signature of the  $\delta^{13}\text{C}_{\text{org}}$  records from  
417 the northern SCS.

418 Fluvial input from Taiwan, especially via submarine canyon systems, makes the northern SCS a depocenter for organic  
419 carbon burial, with important implications for the basin's sedimentary architecture, long-term carbon budget, and even  
420 hydrocarbon source rock potential (Kao et al., 2006). Paleoceanographic records indicate that productivity and organic  
421 carbon burial increased during glacial periods (Thunell et al., 1992), likely driven by nutrient delivery from Taiwan's  
422 sediments that enhanced the biological pump and contributed to regional carbon drawdown. In the modern setting, episodic

423 sediment fluxes during typhoons sustain unusually high chlorophyll-a concentrations in deep SCS waters relative to the  
424 global ocean (Shih et al., 2019). Moreover, northeast monsoon-driven mixing between the China Coastal Current and  
425 Taiwan Strait Current, reinforced by sediment and nutrient inputs dominantly from Taiwan and the Yangtze River, sustains  
426 elevated productivity in the northern SCS (Huang et al., 2020). Collectively, these processes highlight Taiwan's sediment  
427 flux as a key linkage between monsoon forcing, nutrient cycling, and primary production across both modern and in the past.

### 428 **5.3 Influence of climate and monsoon on carbon burial**

429 In the TWFB, carbon geochemistry and gamma-ray data largely reflect the evolution of the foreland basin synchronously  
430 with the shifts in the regional climate regime (Figure 3). During the deposition of the Chinshui Shale in the late Pliocene  
431 (~3.2 to 2.5 Ma), reconstructions for the northwest Pacific show relatively high global sea levels and stable sea-surface  
432 temperatures (Li et al., 2011; Berends et al., 2021). Such conditions favoured the accumulation of fine-grained sediment,  
433 while elevated sea levels deepened the TWFB and promoted offshore depositional environments-both of which are  
434 expressed in the Chinshui Shale (e.g., Nagel et al., 2013; Vaucher et al., 2023b. Greater water depths and increased distance  
435 from the terrestrial sediment sources also enhanced the relative contribution of marine organic matter. The gamma-ray record  
436 of the TWFB strata further reveals depositional cycles related to interactions between EASM and tropical cyclone  
437 precipitation after ~4.92 Ma, with variability expressed at both short-eccentricity and precession frequency bands (Vaucher  
438 et al., 2023b; Hsieh et al., 2023a).

439 During the early Pleistocene, with deposition of the Cholan FormationFm (~2.5–1.95 Ma), global sea level and regional sea-  
440 surface temperatures became markedly more variable (Li et al., 2011; Berends et al., 2021). The continued uplift and  
441 southwest migration of Taiwan promoted the development of shallow-marine depositional environments recorded in the  
442 Cholan FormationFm (e.g., Pan et al., 2015; Vaucher et al., 2021; Vaucher et al., 2023a; Vaucher et al., 2023b). This is  
443 expressed in the gamma-ray and carbon records as an increase in terrestrially sourced, sandstone-rich intervals with high  
444 variability (Figure 3). The enhanced ~~in~~-export of coarser-grained sediment from land to sea is likely related to the onset of  
445 NHG, when repeated sea-level minima promoted clastic delivery to the basin (Vaucher et al., 2021; Vaucher et al., 2023b).

446 In addition, global climate deterioration related to NHG intensified and destabilised the EASM, ~~which would in turn increase~~  
447 ~~sediment supply to the South China Sea~~ (Wan et al., 2006; Wan et al., 2007a). Paleoclimate reconstructions from East Asia  
448 likewise document a strengthening of the EASM during the late Pliocene, generally near ~3.5 Ma (Zhang et al., 2009; Yang  
449 et al., 2018; Yan et al., 2018; Xin et al., 2020; Nie et al., 2014; Hoang et al., 2010). While the causal relationship between  
450 monsoon intensification and NHG remains debated (Zhang et al., 2009; Xin et al., 2020; Wan et al., 2010b; Nie et al.,  
451 2014), long-term global cooling and sea-level fall coupled with intensified monsoon ~~and~~ and tropical cyclone precipitation likely  
452 acted together to amplify sediment export from land to sea (Vaucher et al., 2023b). In the northern SCS, MAR and TOC  
453 values and amplitudes at both ODP sites increased after ~3 Ma, consistent with increased sediment export (Figure 4; Figure  
454 5). Paleoclimate reconstructions from East Asia likewise document a strengthening of the EASM during the late Pliocene,  
455 generally near ~3.5 Ma (Zhang et al., 2009; Yang et al., 2018; Yan et al., 2018; Xin et al., 2020; Nie et al., 2014; Hoang et

456 al., 2010). While the causal relationship between monsoon intensification and NHC remains debated (Zhang et al., 2009; Xin  
457 et al., 2020; Wan et al., 2010b; Nie et al., 2014), long-term global cooling and sea-level fall coupled with intensified  
458 monsoon and tropical cyclone precipitation likely acted together to amplify sediment export from land to sea (Vaucher et al.,  
459 2023b). At the same time,  $\delta^{13}\text{C}_{\text{org}}$  values at ODP Site 1148 increase after  $\sim 3$  Ma, suggesting increasing marine contribution  
460 to organic carbon. This trend is attributed to enhanced marine primary production driven by nutrient enrichment.  
461 Independent evidence for increased marine primary productivity in this interval comes from elevated abundances of  
462 planktonic foraminifera *Neogloboquadrina dutertrei* and higher biogenic silica production (Wang et al., 2005b).

## 463 6 Conclusion

464 Analyses of late-Miocene to early Pleistocene sedimentary and geochemical records from shallow-marine strata of the  
465 Taiwan Western Foreland Basin and deep-sea sediment cores from the northern South China Sea (SCS) provide clear  
466 evidence for shifting pathways of carbon erosion, transport, and burial shaped by the interplay between tectonic forcing,  
467 climate variability, and oceanographic processes.

468 Sediment provenance reveals marked spatial heterogeneity between the continental slope (ODP Site 1146) and the  
469 continental rise (ODP Site 1148), highlighting the influence of tectonic uplift and evolving ocean circulation on sediment  
470 mixing and deposition. Prior to  $\sim 5.4$  Ma, sediment delivery to the northern SCS was dominated by Pearl River discharge.  
471 Taiwan's rapid emergence and erosion at  $\sim 5.4$  Ma supplied large volumes of clastic material to the basin, which is expressed  
472 in sediment provenance records at Site 1148, whereas Site 1146 remained strongly influenced by Eurasian sources. Pearl  
473 River sediments were dispersed along the continental shelf and slope by alongshore and shallow- to intermediate-water  
474 currents but were largely obstructed from reaching deeper water depths by the northward-flowing Kuroshio Current and the  
475 shallow Taiwan Strait.

476 The onset of Northern Hemisphere Glaciation (NHG;  $\sim 3$  Ma) further amplified sediment erosion and export across the basin.  
477 Long-term global cooling and sea-level fall, coupled with enhanced seasonality, drove the intensification of the East Asian  
478 Summer Monsoon. The resulting increase in monsoon rainfall, as well as persistent tropical cyclone activity, drove  
479 synchronous increases in mass-accumulation rate (MAR), magnetic susceptibility, and Ti/Ca values at both ODP sites,  
480 demonstrating the strong climatic imprint on sediment export. In addition, slightly higher  $\delta^{13}\text{C}_{\text{org}}$  values after  $\sim 3$  Ma indicate  
481 a greater marine contribution to organic matter, attributed to enhanced nutrient-driven marine primary production.

482 Organic carbon burial likewise reflects the combined influence of tectonic and climate forcing. At ODP Site 1146, total  
483 organic carbon (TOC) accumulation parallels MAR and is primarily controlled by long-term sea-level fall and NHG  
484 intensification.  $\delta^{13}\text{C}_{\text{org}}$  values indicate that the bulk of organic matter remained marine in origin, with minor terrestrial  
485 contribution linked to Eurasian sediment export rather than to local tectonics Taiwan's orogenesis. At ODP Site 1148, by  
486 contrast, organic carbon burial is closely tied to Taiwan's uplift and erosion. Importantly, TOC scales proportionally with  
487 MAR, implying that organic matter burial was enhanced—not diluted—by high sediment flux. Despite Taiwan's steep relief,

488 rapid tectonic uplift, and frequent typhoon- and monsoon-driven erosion generating exceptional sediment yields,  $\delta^{13}\text{C}_{\text{org}}$   
489 values indicate that most buried organic carbon was marine. This suggests that Taiwan's erosion enhanced nutrient supply,  
490 stimulating coastal primary productivity. Marine organic matter produced in these settings was then redistributed offshore by  
491 turbidity currents through submarine canyon systems, bypassing the shelf and slope and accumulating in deep-sea  
492 depocenters of the northern SCS.

493 Overall, this study highlights the importance of resolving spatial heterogeneities in sedimentary climate archives.  
494 Disentangling the competing influences of tectonics and climate on sediment supply and carbon burial is critical for robust  
495 intercomparison of paleoclimate records, and for reconciling apparent inconsistencies among proxy reconstructions. Our  
496 findings also demonstrate that terrestrial sediment export contributes to carbon drawdown via two distinct pathways: (1)  
497 direct burial of eroded terrestrial organic matter and (2) nutrient supply that fuels marine primary production and subsequent  
498 burial of marine organic matter. This work establishes a direct link between the tectonic evolution of an arc-continent  
499 collisional orogen and changes in carbon storage in adjacent basins, and disentangles the mechanisms by which the erosion  
500 of mid-latitude orogens contributed to long-term carbon sequestration.

## 501 Acknowledgements

502 We would like to thank Dr. Yusuke Kubo at the Japan Agency for Marine-Earth Science and Technology for access to the  
503 ODP Site 1146 and 1148 core samples. This research was supported financially through the Institute of Earth Sciences  
504 Postdoctoral fellowship awarded to A.I. Hsieh from the University of Lausanne. R. Vaucher acknowledges the Swiss  
505 National Science Foundation Postdoc.Mobility Grant (P400P2\_183946) which supported him during data collection from the  
506 Cholan Formation. We express our gratitude to Kuo-Hang Chen for supporting the magnetostratigraphic analysis, Tiffany  
507 Monnier for assisting in sample processing and analysis, and Ling-Wen Liu for elemental and isotope analyses. We are  
508 grateful for the constructive feedback from an anonymous referee and Prof. Shannon Dulin, as well as the support from the  
509 editor, Prof. Lynn Soreghan, who helped to greatly improve this manuscript.

## 510 Conflict of interest

511 The authors declare no conflict of interest

## 512 Author contributions

513 A.I.H. was responsible for the design and conceptualization of this study, supervised by S.J. Data collection was completed  
514 by A.I.H., S.B., and R.V. A.I.H., T.A., L.L., B.B., L.K., and P.-L.W. were responsible for sample analysis. T.A., L.L., S.B.,

515 R.V., and S.J provided support in the interpretation of sedimentary paleoenvironmental proxies. All co-authors reviewed and  
516 approved the manuscript.

517 **Data availability**

518 The data that support the findings of this study can be found on PANGAEA.

519 **References**

520 Aumont, O., Orr, J. C., Monfray, P., Ludwig, W., Amiotte-Suchet, P., and Probst, J.-L.: Riverine-driven interhemispheric  
521 transport of carbon, *Global Biogeochem. Cycles*, 15, 393-405, 10.1029/1999GB001238, 2001.

522 Bayon, G., Patriat, M., Godderis, Y., Trinquier, A., De Deckker, P., Kulhanek, D. K., Holbourn, A., and Rosenthal, Y.:  
523 Accelerated mafic weathering in Southeast Asia linked to late Neogene cooling, *Sci. Adv.*, 9, eadf3141,  
524 doi:10.1126/sciadv.adf3141, 2023.

525 Behar, F., Beaumont, V., and De B. Penteado, H. L.: Rock-Eval 6 Technology: Performances and Developments, *Oil & Gas*  
526 *Science and Technology - Rev. IFP*, 56, 111-134, 10.2516/ogst:2001013, 2001.

527 Berends, C. J., de Boer, B., and van de Wal, R. S. W.: Reconstructing the evolution of ice sheets, sea level, and atmospheric  
528 CO<sub>2</sub> during the past 3.6 million years, *Clim. Past*, 17, 361-377, 10.5194/cp-17-361-2021, 2021.

529 Berner, R. A.: The long-term carbon cycle, fossil fuels and atmospheric composition, *Nature*, 426, 323-326,  
530 10.1038/nature02131, 2003.

531 Bertaz, J., Liu, Z., Colin, C., Dapoigny, A., Lin, A. T.-S., Li, Y., and Jian, Z.: Climatic and Environmental Impacts on the  
532 Sedimentation of the SW Taiwan Margin Since the Last Deglaciation: Geochemical and Mineralogical Investigations,  
533 *Paleoceanogr. Paleoclimatol.*, 39, e2023PA004745, 10.1029/2023PA004745, 2024.

534 Beusen, A. H. W., Bouwman, A. F., Van Beek, L. P. H., Mogollón, J. M., and Middelburg, J. J.: Global riverine N and P  
535 transport to ocean increased during the 20th century despite increased retention along the aquatic continuum,  
536 *Biogeosciences*, 13, 2441-2451, 10.5194/bg-13-2441-2016, 2016.

537 Boulay, S., Colin, C., Trentesaux, A., Frank, N., and Liu, Z.: Sediment sources and East Asian monsoon intensity over the  
538 last 450 ky. Mineralogical and geochemical investigations on South China Sea sediments, *Palaeogeogr. Palaeoclimatol.*  
539 *Palaeoecol.*, 228, 260-277, 10.1016/j.palaeo.2005.06.005, 2005.

540 Burke, K. D., Williams, J. W., Chandler, M. A., Haywood, A. M., Lunt, D. J., and Otto-Bliesner, B. L.: Pliocene and Eocene  
541 provide best analogs for near-future climates, *Proc. Nat. Acad. Sci.*, 115, 13288-13293, 10.1073/pnas.1809600115, 2018.

542 Canadell, J. G., Monteiro, P. M. S., Costa, M. H., Cotrim da Cunha, L., Cox, P. M., Eliseev, A. V., Henson, S., Ishii, M.,  
543 Jaccard, S., Koven, C., Lohila, A., Patra, P. K., Piao, S., Rogelj, J., Syampungani, S., Zaehle, S., and Zickfeld, K.: Global  
544 Carbon and Other Biogeochemical Cycles and Feedbacks, in: *Climate Change 2021: The Physical Science Basis*.

545 Contribution of Working Group I to the Sixth Assessment Report of the Intergovernmental Panel on Climate Change, edited  
546 by: Masson-Delmotte, V., Zhai, P., Pirani, A., Connors, S. L., Péan, C., Berger, S., Caud, N., Chen, Y., Goldfarb, L., Gomis,  
547 M. I., Huang, M., Leitzell, K., Lonnoy, E., Matthews, J. B. R., Maycock, T. K., Waterfield, T., Yelekçi, O., Yu, R., and  
548 Zhou, B., Cambridge University Press, Cambridge, United Kingdom and New York, NY, USA, 673-816,  
549 10.1017/9781009157896.007, 2021.

550 Castelltort, S., Nagel, S., Mouthereau, F., Lin, A. T.-S., Wetzel, A., Kaus, B., Willett, S., Chiang, S.-P., and Chiu, W.-Y.:  
551 Sedimentology of early Pliocene sandstones in the south-western Taiwan foreland: Implications for basin physiography in  
552 the early stages of collision, *J. Asian Earth Sci.*, 40, 52-71, 10.1016/j.jseas.2010.09.005, 2011.

553 Caves, J. K., Jost, A. B., Lau, K. V., and Maher, K.: Cenozoic carbon cycle imbalances and a variable weathering feedback,  
554 *Earth Planet. Sci. Lett.*, 450, 152-163, 10.1016/j.epsl.2016.06.035, 2016.

555 Chen, C.-W., Oguchi, T., Hayakawa, Y. S., Saito, H., Chen, H., Lin, G.-W., Wei, L.-W., and Chao, Y.-C.: Sediment yield  
556 during typhoon events in relation to landslides, rainfall, and catchment areas in Taiwan, *Geomorphology*, 303, 540-548,  
557 10.1016/j.geomorph.2017.11.007, 2018.

558 Chen, J.-M., Li, T., and Shih, C.-F.: Tropical cyclone- and monsoon-induced rainfall variability in Taiwan, *J. Clim.*, 23,  
559 4107-4120, 10.1175/2010jcli3355.1, 2010.

560 Chen, W.-S.: An Introduction to the Geology of Taiwan, Geologic Society of Taiwan, Taipei, Taiwan2016.

561 Cheng, X., Zhao, Q., Wang, J., Jian, Z., Xia, P., Huang, B., Fang, D., Xu, J., Zhou, Z., and Wang, P.: Data Report: Stable  
562 Isotopes from Sites 1147 and 1148, 10.2973/odp.proc.sr.184.223.2004, 2004.

563 Chien, F.-C. and Kuo, H.-C.: On the extreme rainfall of Typhoon Morakot (2009), *J. Geophys. Res.*, 116, D05104,  
564 10.1029/2010jd015092, 2011.

565 Chmura, G. L. and Aharon, P.: Stable carbon isotope signatures of sedimentary carbon in coastal wetlands as indicators of  
566 salinity regime, *J. Coast. Res.*, 11, 124-135, 1995.

567 Cleveland, W. S., Grosse, E., and Shyu, W. M.: Local Regression Models, 1st, Statistical Models in S, Routledge, New  
568 York, 10.1201/9780203738535, 1992.

569 Clift, P. D.: Controls on the erosion of Cenozoic Asia and the flux of clastic sediment to the ocean, *Earth Planet. Sci. Lett.*,  
570 241, 571-580, 10.1016/j.epsl.2005.11.028, 2006.

571 Clift, P. D.: Variations in aridity across the Asia–Australia region during the Neogene and their impact on vegetation, *Geol.  
572 Soc. Lond. Spec. Pub.*, 549, 157-178, 10.1144/SP549-2023-58, 2025.

573 Clift, P. D. and Jonell, T. N.: Himalayan-Tibetan Erosion Is Not the Cause of Neogene Global Cooling, *Geophys. Res. Lett.*,  
574 48, e2020GL087742, 10.1029/2020GL087742, 2021.

575 Clift, P. D., Wan, S., and Blusztajn, J.: Reconstructing chemical weathering, physical erosion and monsoon intensity since  
576 25Ma in the northern South China Sea: A review of competing proxies, *Earth Sci. Rev.*, 130, 86-102,  
577 10.1016/j.earscirev.2014.01.002, 2014.

578 Clift, P. D., Jonell, T. N., Du, Y., and Bornholdt, T.: The impact of Himalayan-Tibetan erosion on silicate weathering and  
579 organic carbon burial, *Chem. Geol.*, 656, 122106, 10.1016/j.chemgeo.2024.122106, 2024a.

580 Clift, P. D., Lee, J. I., Clark, M. K., and Blusztajn, J.: Erosional response of South China to arc rifting and monsoonal  
581 strengthening; a record from the South China Sea, *Mar. Geol.*, 184, 207-226, 10.1016/S0025-3227(01)00301-2, 2002.

582 Clift, P. D., Du, Y., Mohtadi, M., Pahnke, K., Sutorius, M., and Böning, P.: The erosional and weathering response to arc-  
583 continent collision in New Guinea, *J. Geol. Soc.*, 181, jgs2023-2207, 10.1144/jgs2023-207, 2024b.

584 Clift, P. D., Betzler, C., Clemens, S. C., Christensen, B., Eberli, G. P., France-Lanord, C., Gallagher, S., Holbourn, A.,  
585 Kuhnt, W., Murray, R. W., Rosenthal, Y., Tada, R., and Wan, S.: A synthesis of monsoon exploration in the Asian marginal  
586 seas, *Scientific Drilling*, 31, 1-29, 10.5194/sd-31-1-2022, 2022.

587 Covey, M.: The evolution of foreland basins to steady state: Evidence from the western Taiwan foreland basin, in: *Foreland  
588 Basins*, edited by: Allen, P. A., and Homewood, P., Blackwell Publishing Ltd., 77-90, 10.1002/9781444303810.ch4, 1986.

589 Dadson, S. J., Hovius, N., Chen, H., Dade, W. B., Lin, J.-C., Hsu, M.-L., Lin, C.-W., Horng, M.-J., Chen, T.-C., Milliman,  
590 J., and Stark, C. P.: Earthquake-triggered increase in sediment delivery from an active mountain belt, *Geology*, 32,  
591 10.1130/g20639.1, 2004.

592 Dadson, S. J., Hovius, N., Chen, H., Dade, W. B., Hsieh, M.-L., Willett, S. D., Hu, J.-C., Horng, M.-J., Chen, M.-C., Stark,  
593 C. P., Lague, D., and Lin, J.-C.: Links between erosion, runoff variability and seismicity in the Taiwan orogen, *Nature*, 426,  
594 648-651, 10.1038/nature02150, 2003.

595 Dagg, M., Benner, R., Lohrenz, S., and Lawrence, D.: Transformation of dissolved and particulate materials on continental  
596 shelves influenced by large rivers: plume processes, *Cont. Shelf Res.*, 24, 833-858, 10.1016/j.csr.2004.02.003, 2004.

597 Dashtgard, S. E., Löwemark, L., Wang, P.-L., Setiaji, R. A., and Vaucher, R.: Geochemical evidence of tropical cyclone  
598 controls on shallow-marine sedimentation (Pliocene, Taiwan), *Geology*, 49, 566-570, 10.1130/g48586.1, 2021.

599 Dowsett, H. J.: The PRISM palaeoclimate reconstruction and Pliocene sea-surface temperature, in: *Deep-Time Perspectives  
600 on Climate Change: Marrying the Signal from Computer Models and Biological Proxies*, edited by: Williams, M., Haywood,  
601 A. M., Gregory, F. J., and Schmidt, D. N., Geological Society of London, 0, 10.1144/tms002.21, 2007.

602 Dürr, H. H., Meybeck, M., Hartmann, J., Laruelle, G. G., and Roubeix, V.: Global spatial distribution of natural riverine  
603 silica inputs to the coastal zone, *Biogeosciences*, 8, 597-620, 10.5194/bg-8-597-2011, 2011.

604 Espitalie, J., Deroo, G., and Marquis, F.: La pyrolyse Rock-Eval et ses applications. Première partie, *Rev. Inst. Fr. Pét.*, 40,  
605 563-579, 10.2516/ogst:1985035, 1985.

606 Fedorov, A. V., Brierley, C. M., and Emanuel, K.: Tropical cyclones and permanent El Niño in the early Pliocene epoch,  
607 *Nature*, 463, 1066-1070, 10.1038/nature08831, 2010.

608 Fedorov, A. V., Brierley, C. M., Lawrence, K. T., Liu, Z., Dekens, P. S., and Ravelo, A. C.: Patterns and mechanisms of  
609 early Pliocene warmth, *Nature*, 496, 43-49, 10.1038/nature12003, 2013.

610 Froelich, P. N.: Kinetic control of dissolved phosphate in natural rivers and estuaries: A primer on the phosphate buffer  
611 mechanism, *Limnol. Oceanogr.*, 33, 649-668, 10.4319/lo.1988.33.4part2.0649, 1988.

612 Galewsky, J., Stark, C. P., Dadson, S., Wu, C. C., Sobel, A. H., and Horng, M. J.: Tropical cyclone triggering of sediment  
613 discharge in Taiwan, *J. Geophys. Res.*, 111, F03014, 10.1029/2005JF000428, 2006.

614 Galy, V., France-Lanord, C., Beyssac, O., Faure, P., Kudrass, H., and Palhol, F.: Efficient organic carbon burial in the  
615 Bengal fan sustained by the Himalayan erosional system, *Nature*, 450, 407-410, 10.1038/nature06273, 2007.

616 Ge, J., Torres, R., Chen, C., Liu, J., Xu, Y., Bellerby, R., Shen, F., Bruggeman, J., and Ding, P.: Influence of suspended  
617 sediment front on nutrients and phytoplankton dynamics off the Changjiang Estuary: A FVCOM-ERSEM coupled model  
618 experiment, *J. Mar. Syst.*, 204, 103292, 10.1016/j.jmarsys.2019.103292, 2020.

619 GEBCO Compilation Group: GEBCO 2025 Grid, 10.5285/37c52e96-24ea-67ce-e063-7086abc05f29, 2025.

620 Green, W. G. and Fearon, R. E.: Well logging by radioactivity, *Geophysics*, 5, 272-283, 1940.

621 Haq, B. U. and Ogg, J. G.: Retraversing the Highs and Lows of Cenozoic Sea Levels, *GSA Today*, 34, 4-11,  
622 10.1130/GSATGG593A.1, 2024.

623 Haq, B. U., Hardenbol, J., and Vail, P. R.: Chronology of Fluctuating Sea Levels Since the Triassic, *Science*, 235, 1156-  
624 1167, 10.1126/science.235.4793.1156, 1987.

625 Hilton, R. G. and West, A. J.: Mountains, erosion and the carbon cycle, *Nat. Rev. Earth Environ.*, 1, 284-299,  
626 10.1038/s43017-020-0058-6, 2020.

627 Hilton, R. G., Galy, A., Hovius, N., Horng, M.-J., and Chen, H.: The isotopic composition of particulate organic carbon in  
628 mountain rivers of Taiwan, *Geochim. Cosmochim. Acta*, 74, 3164-3181, 10.1016/j.gca.2010.03.004, 2010.

629 Hilton, R. G., Galy, A., Hovius, N., Horng, M.-J., and Chen, H.: Efficient transport of fossil organic carbon to the ocean by  
630 steep mountain rivers: An orogenic carbon sequestration mechanism, *Geology*, 39, 71-74, 10.1130/g31352.1, 2011.

631 Hoang, L. V., Clift, P. D., Schwab, A. M., Huuse, M., Nguyen, D. A., and Zhen, S.: Large-scale erosional response of SE  
632 Asia to monsoon evolution reconstructed from sedimentary records of the Song Hong-Yinggehai and Qiongdongnan basins,  
633 South China Sea, *Geol. Soc. Lond. Spec. Pub.*, 342, 219-244, doi:10.1144/SP342.13, 2010.

634 Holbourn, A., Kuhnt, W., Clemens, S. C., and Heslop, D.: A ~12 Myr Miocene record of East Asian Monsoon variability  
635 from the South China Sea, *Paleoceanogr. Paleoclimatol.*, 36, 10.1029/2021pa004267, 2021.

636 Holbourn, A., Kuhnt, W., Schulz, M., and Erlenkeuser, H.: Impacts of orbital forcing and atmospheric carbon dioxide on  
637 Miocene ice-sheet expansion, *Nature*, 438, 483-487, 10.1038/nature04123, 2005.

638 Holbourn, A., Kuhnt, W., Schulz, M., Flores, J.-A., and Andersen, N.: Orbitally-paced climate evolution during the middle  
639 Miocene “Monterey” carbon-isotope excursion, *Earth Planet. Sci. Lett.*, 261, 534-550, 10.1016/j.epsl.2007.07.026, 2007.

640 Horng, C.-S.: Age of the Tananwan Formation in Northern Taiwan: A reexamination of the magnetostratigraphy and  
641 calcareous nannofossil biostratigraphy, *Terr. Atmos. Ocean Sci.*, 25, 10.3319/tao.2013.11.05.01(tt), 2014.

642 Horng, C.-S. and Huh, C.-A.: Magnetic properties as tracers for source-to-sink dispersal of sediments: A case study in the  
643 Taiwan Strait, *Earth Planet. Sci. Lett.*, 10.1016/j.epsl.2011.07.002, 2011.

644 Hoshiba, Y. and Yamanaka, Y.: Along-coast shifts of plankton blooms driven by riverine inputs of nutrients and fresh water  
645 onto the coastal shelf: a model simulation, *J. Oceanogr.*, 69, 753-767, 10.1007/s10872-013-0206-4, 2013.

646 Houghton, R. A.: Why are estimates of the terrestrial carbon balance so different?, *Glob. Change Biol.*, 9, 500-509,  
647 10.1046/j.1365-2486.2003.00620.x, 2003.

648 Hsieh, A. I., Dashtgard, S. E., Clift, P. D., Lo, L., Vaucher, R., and Löwemark, L.: Competing influence of the Taiwan  
649 orogen and East Asian Summer Monsoon on South China Sea paleoenvironmental proxy records, *Palaeogeogr.  
650 Palaeoclimatol. Palaeoecol.*, 635, 111933, 10.1016/j.palaeo.2023.111933, 2024.

651 Hsieh, A. I., Vaucher, R., Löwemark, L., Dashtgard, S. E., Horng, C. S., Lin, A. T.-S., and Zeeden, C.: Influence of a rapidly  
652 uplifting orogen on the preservation of climate oscillations, *Paleoceanogr. Paleoclimatol.*, 38, e2022PA004586,  
653 10.1029/2022PA004586, 2023a.

654 Hsieh, A. I., Dashtgard, S. E., Wang, P. L., Horng, C. S., Su, C. C., Lin, A. T., Vaucher, R., and Löwemark, L.: Multi-proxy  
655 evidence for rapidly shifting sediment sources to the Taiwan Western Foreland Basin at the Miocene–Pliocene transition,  
656 *Basin Res.*, 35, 932-948, 10.1111/bre.12741, 2023b.

657 Hsieh, A. I., Vaucher, R., MacEachern, J. A., Zeeden, C., Huang, C., Lin, A. T., Löwemark, L., and Dashtgard, S. E.:  
658 Resolving allogenic forcings on shallow-marine sedimentary archives of the Taiwan Western Foreland Basin,  
659 *Sedimentology*, 72, 1755-1785, 10.1111/sed.70020, 2025.

660 Hu, D., Böning, P., Köhler, C. M., Hillier, S., Pressling, N., Wan, S., Brumsack, H. J., and Clift, P. D.: Deep sea records of  
661 the continental weathering and erosion response to East Asian monsoon intensification since 14 ka in the South China Sea,  
662 *Chem. Geol.*, 326-327, 1-18, 10.1016/j.chemgeo.2012.07.024, 2012.

663 Hu, J., Kawamura, H., Li, C., Hong, H., and Jiang, Y.: Review on current and seawater volume transport through the Taiwan  
664 Strait, *J. Oceanogr.*, 66, 591-610, 10.1007/s10872-010-0049-1, 2010.

665 Hu, Z., Huang, B., Geng, L., and Wang, N.: Sediment provenance in the Northern South China Sea since the Late Miocene,  
666 *Open Geosci.*, 14, 454, 10.1515/geo-2022-0454, 2022.

667 Huang, T.-H., Chen, C.-T. A., Bai, Y., and He, X.: Elevated primary productivity triggered by mixing in the quasi-cul-de-sac  
668 Taiwan Strait during the NE monsoon, *Sci. Rep.*, 10, 7846, 10.1038/s41598-020-64580-6, 2020.

669 Jagoutz, O., Macdonald, F. A., and Royden, L.: Low-latitude arc–continent collision as a driver for global cooling, *Proc. Nat.  
670 Acad. Sci.*, 113, 4935-4940, 10.1073/pnas.1523667113, 2016.

671 Jakob, K. A., Wilson, P. A., Pross, J., Ezard, T. H. G., Fiebig, J., Repschläger, J., and Friedrich, O.: A new sea-level record  
672 for the Neogene/Quaternary boundary reveals transition to a more stable East Antarctic Ice Sheet, *Proc. Nat. Acad. Sci.*, 117,  
673 30980-30987, doi:10.1073/pnas.2004209117, 2020.

674 Janapati, J., Seela, B. K., Lin, P.-L., Wang, P. K., and Kumar, U.: An assessment of tropical cyclones rainfall erosivity for  
675 Taiwan, *Sci. Rep.*, 9, 15862, 10.1038/s41598-019-52028-5, 2019.

676 Jin, L., Shan, X., Vaucher, R., Qiao, S., Wang, C., Liu, S., Wang, H., Fang, X., Bai, Y., Zhu, A., and Shi, X.: Sea-level  
677 changes control coastal organic carbon burial in the East China Sea during the late MIS 3, *Earth Planet. Sci. Lett.*, 229,  
678 104225, 10.1016/j.gloplacha.2023.104225, 2023.

679 Kämpf, N. and Schwertmann, U.: Goethite and hematite in a climosequence in southern Brazil and their application in  
680 classification of kaolinitic soils, *Geoderma*, 29, 27-39, 10.1016/0016-7061(83)90028-9, 1983.

681 Kao, S.-J., Shiah, F.-K., Wang, C.-H., and Liu, K.-K.: Efficient trapping of organic carbon in sediments on the continental  
682 margin with high fluvial sediment input off southwestern Taiwan, *Cont. Shelf Res.*, 26, 2520-2537,  
683 10.1016/j.csr.2006.07.030, 2006.

684 Kao, S. J. and Milliman, J. D.: Water and sediment discharge from small mountainous rivers, Taiwan: The roles of lithology,  
685 episodic events, and human activities, *J. Geol.*, 116, 431-448, 10.1086/590921, 2008.

686 Kissel, C., Liu, Z., Li, J., and Wandres, C.: Magnetic minerals in three Asian rivers draining into the South China Sea: Pearl,  
687 Red, and Mekong Rivers, *Geochem. Geophys. Geosyst.*, 17, 1678-1693, 10.1002/2016GC006283, 2016.

688 Kissel, C., Liu, Z., Li, J., and Wandres, C.: Magnetic signature of river sediments drained into the southern and eastern part  
689 of the South China Sea (Malay Peninsula, Sumatra, Borneo, Luzon and Taiwan), *Sediment. Geol.*, 347, 10-20,  
690 10.1016/j.sedgeo.2016.11.007, 2017.

691 Krumins, V., Gehlen, M., Arndt, S., Van Cappellen, P., and Regnier, P.: Dissolved inorganic carbon and alkalinity fluxes  
692 from coastal marine sediments: model estimates for different shelf environments and sensitivity to global change,  
693 *Biogeosciences*, 10, 371-398, 10.5194/bg-10-371-2013, 2013.

694 Lee, T.-Y., Huang, J.-C., Lee, J.-Y., Jien, S.-H., Zehetner, F., and Kao, S.-J.: Magnified sediment export of small  
695 mountainous rivers in Taiwan: Chain reactions from increased rainfall intensity under global warming, *PLoS One*, 10,  
696 e0138283, 10.1371/journal.pone.0138283, 2015.

697 Li, B., Wang, J., Huang, B., Li, Q., Jian, Z., Zhao, Q., Su, X., and Wang, P.: South China Sea surface water evolution over  
698 the last 12 Myr: A south-north comparison from Ocean Drilling Program Sites 1143 and 1146, *Paleoceanography*, 19,  
699 PA1009, 10.1029/2003PA000906, 2004.

700 Li, L., Li, Q., Tian, J., Wang, P., Wang, H., and Liu, Z.: A 4-Ma record of thermal evolution in the tropical western Pacific  
701 and its implications on climate change, *Earth Planet. Sci. Lett.*, 309, 10-20, 10.1016/j.epsl.2011.04.016, 2011.

702 Li, M., Wan, S., Colin, C., Jin, H., Zhao, D., Pei, W., Jiao, W., Tang, Y., Tan, Y., Shi, X., and Li, A.: Expansion of C4 plants  
703 in South China and evolution of East Asian monsoon since 35 Ma: Black carbon records in the northern South China Sea,  
704 *Global Planet. Change*, 223, 104079, 10.1016/j.gloplacha.2023.104079, 2023.

705 Li, X.-h., Wei, G., Shao, L., Liu, Y., Liang, X., Jian, Z., Sun, M., and Wang, P.: Geochemical and Nd isotopic variations in  
706 sediments of the South China Sea: a response to Cenozoic tectonism in SE Asia, *Earth Planet. Sci. Lett.*, 211, 207-220,  
707 10.1016/S0012-821X(03)00229-2, 2003.

708 Lin, A. T.-S. and Watts, A. B.: Origin of the West Taiwan basin by orogenic loading and flexure of a rifted continental  
709 margin, *Journal of Geophysical Research: Solid Earth*, 107, ETG 2-1-ETG 2-19, 10.1029/2001jb000669, 2002.

710 Lin, H.-T., Yang, J.-I., Wu, Y.-T., Shiau, Y.-J., Lo, L., and Yang, S.-H.: The spatiotemporal variations of marine nematode  
711 populations may serve as indicators of changes in marine ecosystems, *Mar. Pollut. Bull.*, 211, 117373,  
712 10.1016/j.marpolbul.2024.117373, 2025.

713 Lisiecki, L. E. and Raymo, M. E.: A Pliocene-Pleistocene stack of 57 globally distributed benthic  $\delta^{18}\text{O}$  records,  
714 Paleoceanography, 20, PA1003, 10.1029/2004pa001071, 2005.

715 Liu, J., Chen, Z., Chen, M., Yan, W., Xiang, R., and Tang, X.: Magnetic susceptibility variations and provenance of surface  
716 sediments in the South China Sea, Sediment. Geol., 230, 77-85, 10.1016/j.sedgeo.2010.07.001, 2010a.

717 Liu, J. P., Liu, C. S., Xu, K. H., Milliman, J. D., Chiu, J. K., Kao, S. J., and Lin, S. W.: Flux and fate of small mountainous  
718 rivers derived sediments into the Taiwan Strait, Mar. Geol., 256, 65-76, 10.1016/j.margeo.2008.09.007, 2008.

719 Liu, J. P., Xue, Z., Ross, K., Wang, H. J., Yang, Z. S., Li, A. C., and Gao, S.: Fate of sediments delivered to the sea by Asian  
720 large rivers: Long-distance transport and formation of remote alongshore clinotherms, Sed. Record, 7, 4-9, 10.2110/  
721 sedred.2009.4.4, 2009a.

722 Liu, J. T., Kao, S. J., Huh, C. A., and Hung, C. C.: Gravity flows associated with flood events and carbon burial: Taiwan as  
723 instructional source area, Annu. Rev. Mar. Sci., 5, 47-68, 10.1146/annurev-marine-121211-172307, 2013.

724 Liu, J. T., Wang, Y.-H., Yang, R. J., Hsu, R. T., Kao, S.-J., Lin, H.-L., and Kuo, F. H.: Cyclone-induced hyperpycnal  
725 turbidity currents in a submarine canyon, J. Geophys. Res. [Oceans], 117, C04033, 10.1029/2011jc007630, 2012.

726 Liu, J. T., Hung, J.-J., Lin, H.-L., Huh, C.-A., Lee, C.-L., Hsu, R. T., Huang, Y.-W., and Chu, J. C.: From suspended  
727 particles to strata: The fate of terrestrial substances in the Gaoping (Kaoping) submarine canyon, J. Mar. Syst., 76, 417-432,  
728 10.1016/j.jmarsys.2008.01.010, 2009b.

729 Liu, Z., Alain, T., Clemens, S. C., and Wang, P.: Quaternary clay mineralogy in the northern South China Sea (ODP Site  
730 1146), Science in China Series D: Earth Sciences, 46, 1223-1235, 10.1360/02yd0107, 2003.

731 Liu, Z., Zhao, Y., Colin, C., Siringan, F. P., and Wu, Q.: Chemical weathering in Luzon, Philippines from clay mineralogy  
732 and major-element geochemistry of river sediments, Appl. Geochem., 24, 2195-2205, 10.1016/j.apgeochem.2009.09.025,  
733 2009c.

734 Liu, Z., Colin, C., Huang, W., Le, K. P., Tong, S., Chen, Z., and Trentesaux, A.: Climatic and tectonic controls on  
735 weathering in south China and Indochina Peninsula: Clay mineralogical and geochemical investigations from the Pearl, Red,  
736 and Mekong drainage basins, Geochem. Geophys. Geosyst., 8, Q05005, 10.1029/2006gc001490, 2007.

737 Liu, Z., Colin, C., Li, X., Zhao, Y., Tuo, S., Chen, Z., Siringan, F. P., Liu, J. T., Huang, C.-Y., You, C.-F., and Huang, K.-F.:  
738 Clay mineral distribution in surface sediments of the northeastern South China Sea and surrounding fluvial drainage basins:  
739 Source and transport, Mar. Geol., 277, 48-60, 10.1016/j.margeo.2010.08.010, 2010b.

740 Liu, Z., Zhao, Y., Colin, C., Stattegger, K., Wiesner, M. G., Huh, C.-A., Zhang, Y., Li, X., Sompongchaiyakul, P., You, C.-  
741 F., Huang, C.-Y., Liu, J. T., Siringan, F. P., Le, K. P., Sathiamurthy, E., Hantoro, W. S., Liu, J., Tuo, S., Zhao, S., Zhou, S.,  
742 He, Z., Wang, Y., Bunsomboonsakul, S., and Li, Y.: Source-to-sink transport processes of fluvial sediments in the South  
743 China Sea, Earth Sci. Rev., 153, 238-273, 10.1016/j.earscirev.2015.08.005, 2016.

744 Lüdmann, T., Wong, H. K., and Berglar, K.: Upward flow of North Pacific Deep Water in the northern South China Sea as  
745 deduced from the occurrence of drift sediments, Geophys. Res. Lett., 32, 1-4, 10.1029/2004GL021967, 2005.

746 Luo, X., Zhou, H., Satriawan, T. W., Tian, J., Zhao, R., Keenan, T. F., Griffith, D. M., Sitch, S., Smith, N. G., and Still, C.  
747 J.: Mapping the global distribution of C4 vegetation using observations and optimality theory, *Nat. Commun.*, 15, 1219,  
748 10.1038/s41467-024-45606-3, 2024.

749 Lurcock, P. C. and Wilson, G. S.: PuffinPlot: A versatile, user-friendly program for paleomagnetic analysis, *Geochem.*  
750 *Geophys. Geosyst.*, 13, Q06Z45, 10.1029/2012GC004098, 2012.

751 Macdonald, F. A., Swanson-Hysell, N. L., Park, Y., Lisiecki, L., and Jagoutz, O.: Arc-continent collisions in the tropics set  
752 Earth's climate state, *Science*, 364, 181-184, 10.1126/science.aav5300, 2019.

753 Maher, B. A.: Characterisation of soils by mineral magnetic measurements, *Phys. Earth Planet. Inter.*, 42, 76-92,  
754 10.1016/S0031-9201(86)8010-3, 1986.

755 Martiny, A. C., Pham, C. T. A., Primeau, F. W., Vrugt, J. A., Moore, J. K., Levin, S. A., and Lomas, M. W.: Strong  
756 latitudinal patterns in the elemental ratios of marine plankton and organic matter, *Nat. Geosci.*, 6, 279-283,  
757 10.1038/ngeo1757, 2013.

758 Miller, K. G., Browning, J. V., Schmelz, W. J., Kopp, R. E., Mountain, G. S., and Wright, J. D.: Cenozoic sea-level and  
759 cryospheric evolution from deep-sea geochemical and continental margin records, *Sci. Adv.*, 6, eaaz1346,  
760 10.1126/sciadv.aaz1346, 2020.

761 Milliman, J. D. and Kao, S.-J.: Hyperpycnal discharge of fluvial sediment to the ocean: Impact of super-typhoon Herb  
762 (1996) on Taiwanese rivers, *J. Geol.*, 113, 503-516, 10.1086/431906, 2005.

763 Milliman, J. D. and Syvitski, J. P. M.: Geomorphic/tectonic control of sediment discharge to the ocean: The importance of  
764 small mountainous rivers, *J. Geol.*, 100, 525-544, 10.1086/629606, 1992.

765 Milliman, J. D., Lee, T. Y., Huang, J. C., and Kao, S. J.: Impact of catastrophic events on small mountainous rivers:  
766 Temporal and spatial variations in suspended- and dissolved-solid fluxes along the Choshui River, central western Taiwan,  
767 during typhoon Mindulle, July 2-6, 2004, *Geochim. Cosmochim. Acta*, 205, 272-294, 10.1016/j.gca.2017.02.015, 2017.

768 Nagel, S., Granjeon, D., Willett, S., Lin, A. T.-S., and Castelltort, S.: Stratigraphic modeling of the Western Taiwan foreland  
769 basin: Sediment flux from a growing mountain range and tectonic implications, *Mar. Pet. Geol.*, 96, 331-347,  
770 10.1016/j.marpetgeo.2018.05.034, 2018.

771 Nagel, S., Castelltort, S., Wetzel, A., Willett, S. D., Mouthereau, F., and Lin, A. T.: Sedimentology and foreland basin  
772 paleogeography during Taiwan arc continent collision, *J. Asian Earth Sci.*, 62, 180-204, 10.1016/j.jseas.2012.09.001, 2013.

773 Nie, J., Stevens, T., Song, Y., King, J. W., Zhang, R., Ji, S., Gong, L., and Cares, D.: Pacific freshening drives Pliocene  
774 cooling and Asian monsoon intensification, *Sci. Rep.*, 4, 5474, 10.1038/srep05474, 2014.

775 Pan, T.-Y., Lin, A. T.-S., and Chi, W.-R.: Paleoenvironments of the evolving Pliocene to early Pleistocene foreland basin in  
776 northwestern Taiwan: An example from the Dahan River section, *Isl. Arc.*, 24, 317-341, 10.1111/iar.12113, 2015.

777 Peterson, B. J. and Fry, B.: Stable isotopes in ecosystem studies, *Annu. Rev. Ecol. Evol. Syst.*, 18, 293-320,  
778 10.1146/annurev.es.18.110187.001453, 1987.

779 Raymo, M. E. and Ruddiman, W. F.: Tectonic forcing of late Cenozoic climate, *Nature*, 359, 117-122, 10.1038/359117a0,  
780 1992.

781 Robinson, M. M., Dowsett, H. J., and Chandler, M. A.: Pliocene role in assessing future climate impacts, *Eos*, 89, 501-502,  
782 10.1029/2008EO490001, 2008.

783 Rohling, E. J., Foster, G. L., Grant, K. M., Marino, G., Roberts, A. P., Tamisiea, M. E., and Williams, F.: Sea-level and  
784 deep-sea-temperature variability over the past 5.3 million years, *Nature*, 508, 477-482, 10.1038/nature13230, 2014.

785 Schlumberger: Log Interpretation Principles/Applications, Schlumberger, Houston, 233 pp.1989.

786 Shao, L., Li, X., Wei, G., Liu, Y., and Fang, D.: Provenance of a prominent sediment drift on the northern slope of the South  
787 China Sea, *Science in China Series D: Earth Sciences*, 44, 919-925, 10.1007/BF02907084, 2001.

788 Shao, L., Qiao, P.-J., Pang, X., Wei, G.-J., Li, Q.-Y., Miao, W.-L., and Li, A.: Nd isotopic variations and its implications in  
789 the recent sediments from the northern South China Sea, *Chin. Sci. Bull.*, 54, 311-317, 10.1007/s11434-008-0453-8, 2009.

790 Shea, K.-S. and Huang, T.: Tertiary stratigraphy in Taiwan, *The Taiwan Mining Industry*, 55, 17-32, 2003.

791 Shih, Y.-Y., Lin, H.-H., Li, D., Hsieh, H.-H., Hung, C.-C., and Chen, C.-T. A.: Elevated carbon flux in deep waters of the  
792 South China Sea, *Sci. Rep.*, 9, 1496, 10.1038/s41598-018-37726-w, 2019.

793 Spangenberg, J. E.: Bulk C, H, O, and fatty acid C stable isotope analyses for purity assessment of vegetable oils from the  
794 southern and northern hemispheres, *Rapid Commun. Mass Spectrom.*, 30, 2447-2461, 10.1002/rcm.7734, 2016.

795 Stepanauskas, R., JØrgensen, N. O. G., Eigaard, O. R., Žvikas, A., Tranvik, L. J., and Leonardson, L.: Summer inputs of  
796 riverine nutrients to the Baltic Sea: Bioavailability and eutrophication relevance, *Ecol. Monogr.*, 72, 579-597, 10.1890/0012-  
797 9615(2002)072[0579:SIORNT]2.0.CO;2, 2002.

798 Still, C., Berry, J., Collatz, G., and Defries, R.: Global distribution of C3 and C4 vegetation: Carbon cycle implications,  
799 *Global Biogeochem. Cycles*, 17, 6-1, 10.1029/2001GB001807, 2003.

800 Teng, L. S., Wang, Y., Tang, C.-H., Huang, C.-Y., Huang, T.-C., Yu, M.-S., and Ke, A.: Tectonic aspects of the Paleogene  
801 depositional basin of northern Taiwan, *Proc. Geol. Soc. China*, 34, 313-336, 1991.

802 Thunell, R. C., Qingmin, M., Calvert, S. E., and Pedersen, T. F.: Glacial-Holocene Biogenic Sedimentation Patterns in the  
803 South China Sea: Productivity Variations and Surface Water pCO<sub>2</sub>, *Paleoceanography*, 7, 143-162, 10.1029/92PA00278,  
804 1992.

805 Tian, J., Wang, P., Cheng, X., and Li, Q.: Establishment of the Plio-Pleistocene astronomical timescale of ODP site 1143,  
806 Southern South China Sea, *Journal of China University of Geosciences*, 30, 31-39, 2005.

807 Tian, J., Xie, X., Ma, W., Jin, H., and Wang, P.: X-ray fluorescence core scanning records of chemical weathering and  
808 monsoon evolution over the past 5 Myr in the southern South China Sea, *Paleoceanography*, 26, 10.1029/2010PA002045,  
809 2011.

810 Tian, J., Zhao, Q., Wang, P., Li, Q., and Cheng, X.: Astronomically modulated Neogene sediment records from the South  
811 China Sea, *Paleoceanography*, 23, 10.1029/2007PA001552, 2008.

812 Tierney, J. E., Haywood, A. M., Feng, R., Bhattacharya, T., and Otto-Bliesner, B. L.: Pliocene warmth consistent with  
813 greenhouse gas forcing, *Geophys. Res. Lett.*, 46, 9136-9144, 10.1029/2019gl083802, 2019.

814 Tory, K. J. and Frank, W. M.: Tropical Cyclone Formation, in: *Global Perspectives on Tropical Cyclones*, 55-91,  
815 10.1142/9789814293488\_0002, 2010.

816 Van Oost, K., Verstraeten, G., Doetterl, S., Notebaert, B., Wiaux, F., Broothaerts, N., and Six, J.: Legacy of human-induced  
817 C erosion and burial on soil-atmosphere C exchange, *Proc. Nat. Acad. Sci.*, 109, 19492-19497, 10.1073/pnas.1211162109,  
818 2012.

819 Vaucher, R., Dillinger, A., Hsieh, A. I., Chi, W.-R., Löwemark, L., and Dashtgard, S. E.: Storm-flood-dominated delta  
820 succession in the Pleistocene Taiwan Strait, *The Depositional Record*, 00, 1-24, 10.1002/dep2.231, 2023a.

821 Vaucher, R., Zeeden, C., Hsieh, A. I., Kaboth-Bahr, S., Lin, A. T., Horng, C.-S., and Dashtgard, S. E.: Hydroclimate  
822 dynamics during the Plio-Pleistocene transition in the northwest Pacific realm, *Global Planet. Change*, 223, 104088,  
823 10.1016/j.gloplacha.2023.104088, 2023b.

824 Vaucher, R., Dashtgard, S. E., Horng, C. S., Zeeden, C., Dillinger, A., Pan, Y. Y., Setiaji, R. A., Chi, W. R., and Lowemark,  
825 L.: Insolation-paced sea level and sediment flux during the early Pleistocene in Southeast Asia, *Sci. Rep.*, 11, 16707,  
826 10.1038/s41598-021-96372-x, 2021.

827 Walker, J. C. G., Hays, P. B., and Kasting, J. F.: A negative feedback mechanism for the long-term stabilization of Earth's  
828 surface temperature, *J. Geophys. Res. [Oceans]*, 86, 9776-9782, 10.1029/JC086iC10p09776, 1981.

829 Wan, S., Li, A., Clift, P. D., and Jiang, H.: Development of the East Asian summer monsoon: Evidence from the sediment  
830 record in the South China Sea since 8.5 Ma, *Palaeogeogr. Palaeoclimatol. Palaeoecol.*, 241, 139-159,  
831 10.1016/j.palaeo.2006.06.013, 2006.

832 Wan, S., Li, A., Clift, P. D., and Stuut, J.-B. W.: Development of the East Asian monsoon: Mineralogical and  
833 sedimentologic records in the northern South China Sea since 20 Ma, *Palaeogeogr. Palaeoclimatol. Palaeoecol.*, 254, 561-  
834 582, 10.1016/j.palaeo.2007.07.009, 2007a.

835 Wan, S., Clift, P. D., Li, A., Li, T., and Yin, X.: Geochemical records in the South China Sea: implications for East Asian  
836 summer monsoon evolution over the last 20 Ma, *Geol. Soc. Lond. Spec. Pub.*, 342, 245-263, doi:10.1144/SP342.14, 2010a.

837 Wan, S., Tian, J., Steinke, S., Li, A., and Li, T.: Evolution and variability of the East Asian summer monsoon during the  
838 Pliocene: Evidence from clay mineral records of the South China Sea, *Palaeogeogr. Palaeoclimatol. Palaeoecol.*, 293, 237-  
839 247, 10.1016/j.palaeo.2010.05.025, 2010b.

840 Wan, S., Li, A., Clift, P. D., Wu, S., Xu, K., and Li, T.: Increased contribution of terrigenous supply from Taiwan to the  
841 northern South China Sea since 3Ma, *Mar. Geol.*, 278, 115-121, 10.1016/j.margeo.2010.09.008, 2010c.

842 Wan, S. M., Li, A. C., Jan-Berend, W. S., and Xu, F. J.: Grain-size records at ODP site 1146 from the northern South China  
843 Sea: Implications on the East Asian monsoon evolution since 20 Ma, *Science in China Series D: Earth Sciences*, 50, 1536-  
844 1547, 10.1007/s11430-007-0082-0, 2007b.

845 Wang, H., Lu, H., Zhao, L., Zhang, H., Lei, F., and Wang, Y.: Asian monsoon rainfall variation during the Pliocene forced  
846 by global temperature change, *Nat. Commun.*, 10, 5272, 10.1038/s41467-019-13338-4, 2019.

847 Wang, P., Prell, W. L., Blum, P., and Party, S. S.: Site 1148, 1-121, 10.2973/odp.proc.ir.184.109.2000, 2000a.

848 Wang, P., Prell, W. L., Blum, P., and Party, S. S.: Site 1146, 1-101, doi:10.2973/odp.proc.ir.184.108.2000, 2000b.

849 Wang, P., Prell, W. L., Blum, P., and Shipboard Scientific, P.: Magnetic susceptibility on ODP Hole 184-1146C,  
850 PANGAEA [dataset], 10.1594/PANGAEA.266354, 2005a.

851 Wang, P., Clemens, S., Beaufort, L., Braconnot, P., Ganssen, G., Jian, Z., Kershaw, P., and Sarnthein, M.: Evolution and  
852 variability of the Asian monsoon system: state of the art and outstanding issues, *Quat. Sci. Rev.*, 24, 595-629,  
853 10.1016/j.quascirev.2004.10.002, 2005b.

854 Wang, R. and Ma, L.: Climate-driven C4 plant distributions in China: divergence in C4 taxa, *Sci. Rep.*, 6, 27977,  
855 10.1038/srep27977, 2016.

856 Westerhold, T., Marwan, N., Drury, A. J., Liebrand, D., Agnini, C., Anagnostou, E., Barnet, J. S. K., Bohaty, S. M., De  
857 Vleeschouwer, D., Florindo, F., Frederichs, T., Hodell, D. A., Holbourn, A. E., Kroon, D., Lauretano, V., Littler, K.,  
858 Lourens, L. J., Lyle, M., Pälike, H., Röhl, U., Tian, J., Wilkens, R. H., Wilson, P. A., and Zachos, J. C.: An astronomically  
859 dated record of Earth's climate and its predictability over the last 66 million years, *Science*, 369, 1383-1388,  
860 10.1126/science.aba6853, 2020.

861 Wilkens, R. H., Westerhold, T., Drury, A. J., Lyle, M., Gorgas, T., and Tian, J.: Revisiting the Ceara Rise, equatorial  
862 Atlantic Ocean: isotope stratigraphy of ODP Leg 154 from 0 to 5 Ma, *Clim. Past*, 13, 779-793, 10.5194/cp-13-779-2017,  
863 2017.

864 Xin, S., Shen, J., Zhang, W., Sun, W., and Xiao, X.: East Asian winter monsoon evolution since the late Pliocene based on a  
865 pollen record from Lake Xingkai, northeast Asia, *Quat. Res.*, 93, 40-59, 10.1017/qua.2019.45, 2020.

866 Xue, J., Chen, J., Li, Y., Huo, J., Zhao, Z., Liu, Y., and Chen, M.: Expansion of C4 plants in the tropical Leizhou Peninsula  
867 during the Last Glacial Maximum: Modulating effect of regional sea-level change, *Sci. Tot. Environ.*, 952, 175897,  
868 10.1016/j.scitotenv.2024.175897, 2024.

869 Yan, Q., Zhang, Z., and Zhang, R.: Investigating sensitivity of East Asian monsoon to orbital forcing during the late Pliocene  
870 Warm Period, *J. Geophys. Res. [Atmos.]*, 10.1029/2017jd027646, 2018.

871 Yan, Q., Wei, T., Zhang, Z., and Jiang, N.: Orbitally induced variation of tropical cyclone genesis potential over the western  
872 North Pacific during the mid-Piacenzian Warm Period: A modeling perspective, *Paleoceanogr. Paleoclimatol.*, 34, 902-916,  
873 10.1029/2018pa003535, 2019.

874 Yan, Q., Wei, T., Korty, R. L., Kossin, J. P., Zhang, Z., and Wang, H.: Enhanced intensity of global tropical cyclones during  
875 the mid-Pliocene warm period, *Proc. Nat. Acad. Sci.*, 113, 12963-12967, 10.1073/pnas.1608950113, 2016.

876 Yang, S., Ding, Z., Feng, S., Jiang, W., Huang, X., and Guo, L.: A strengthened East Asian Summer Monsoon during  
877 Pliocene warmth: Evidence from 'red clay' sediments at Pianguan, northern China, *J. Asian Earth Sci.*, 155, 124-133,  
878 10.1016/j.jseaes.2017.10.020, 2018.

879 Yin, S., Hernández-Molina, F. J., Lin, L., He, M., Gao, J., and Li, J.: Plate convergence controls long-term full-depth  
880 circulation of the South China Sea, *Mar. Geol.*, 459, 107050, 10.1016/j.margeo.2023.107050, 2023.

881 Yu, H.-S., Chiang, C.-S., and Shen, S.-M.: Tectonically active sediment dispersal system in SW Taiwan margin with  
882 emphasis on the Gaoping (Kaoping) Submarine Canyon, *J. Mar. Syst.*, 76, 369-382, 10.1016/j.jmarsys.2007.07.010, 2009.

883 Zhang, Y., Liu, Z., Zhao, Y., Wang, W., Li, J., and Xu, J.: Mesoscale eddies transport deep-sea sediments, *Sci. Rep.*, 4,  
884 5937-5937, 10.1038/srep05937, 2014.

885 Zhang, Y. G., Ji, J., Balsam, W., Liu, L., and Chen, J.: Mid-Pliocene Asian monsoon intensification and the onset of  
886 Northern Hemisphere glaciation, *Geology*, 37, 599-602, 10.1130/g25670a.1, 2009.

887 Zhao, Y., Liu, Z., Zhang, Y., Li, J., Wang, M., Wang, W., and Xu, J.: In situ observation of contour currents in the northern  
888 South China Sea: Applications for deepwater sediment transport, *Earth Planet. Sci. Lett.*, 430, 477-485,  
889 10.1016/j.epsl.2015.09.008, 2015.

890 Zheng, L.-W., Ding, X., Liu, J. T., Li, D., Lee, T.-Y., Zheng, X., Zheng, Z., Xu, M. N., Dai, M., and Kao, S.-J.: Isotopic  
891 evidence for the influence of typhoons and submarine canyons on the sourcing and transport behavior of biospheric organic  
892 carbon to the deep sea, *Earth Planet. Sci. Lett.*, 465, 103-111, 10.1016/j.epsl.2017.02.037, 2017.

893